DEVELOPMENT OF ANALYTICAL TECHNIQUE FOR PLANT SACCHARIDES USING RAMAN SPECTROSCOPY

A Thesis for the degree

of

Doctor of science

Submitted to

School of Science, Kwansei Gakuin University

By

Anggara Mahardika

in October 2018

Abstract

The overall aim of this study is to develop a new technology to study seaweeds for the improvement of aquaculture productivity. Indonesia is one of the top producers of seaweed in the world. The red macrophytic alga, *Kappaphycus alvarezii* is the main source seaweed for the industrial production of *kappa* type carrageenan. The quality of seaweed harvests has become paramount to obtaining good quality of carrageenan. A good quality of seaweed *K. alvarezii* containing about 40-50% of carrageenan. However, instability of environmental conditions may make it difficult to produce good quality carrageenan. Furthermore, harvests are often limited by seaweed diseases, one of the major problems in seaweed farming. *Ice–ice* is the most famous seaweed disease caused by bacterial pathogens. *Ice–ice* disease causes whitening of algae thallus and leads to fragmentation and eventually loss of biomass. Bacterial infection in the algal body often involves degradation of algal storage compounds by bacterial enzymes. To monitor and investigate the bacterial infection in seaweed body, low cost and effective analytical tools are needed. In this study, we demonstrated the ability of combining Raman spectroscopy with chemometric analysis to investigate infective enzymatic activities in seaweed body. A low cost Partial Least Square Regression (PLSR) model with reduced number of test samples was successfully achieved for quantifying the enzymatic reaction mixture with substrate and product in the alfa-amylases activity. In order to qualify of seaweed harvest, imaging Raman spectroscopy (iRs) was successfully used to observe carrageenan content in three different hierarchies of seaweed branches. Furthermore, low cost PLSR model and iRs were successfully used to investigate the carrageenan degradation activities of infected *K. alvarezii* by measuring the decrease in carrageenan content, as a substrate in bacterial enzymatic reaction. From this study, it can be concluded that iRs combined with chemometric analysis is a powerful tool to monitor conditions of seaweed quality.

Contents

Introduction

Background

The general purpose of this study is to develop a new research technology to study reactions in marine algae and interactions between the algae and bacteria, which cause seaweed disease. The development of an accurate and effective technique was motivated in order to solve the problems in seaweed farming caused by the effect of the surrounding environment, such as bacterial infection.

Indonesia is one of the top seaweed producing countries in the world with the national seaweed production capacity up to 10 million tons in 2014 (FAO, 2016). Red algal seaweed *K. alvarezii* is an abundant and important commodity in Indonesia (Ask, 2001). Indonesia is a tropical archipelago that has many potential areas for seaweed farming. There are four largest seaweed farming areas in Indonesia: Karimujawa, Sulawesi, Bali, and Sumba (Soegiarto and Sulustijo, 1990; Manuhara et al. 2016). Seaweed *K. alvarezii* is a major source of industrial use of *kappa* type carrageenan.

Carrageenan

Carrageenan is a sulfated linear polysaccharide accumulated in Rhodophyceae (Normah and Nazarifah, 2003). The *kappa* carrageenan consists of D-galactose-4-sulfate and 3,6 anhydrous D-galactose residues linked with the β (1,4) and α (1,3) carbon bonds. Sulfate accounts for about 20%–35% of the molecular weight (fig. 1; Lechat et al. 1997; campo et al. 2009; Necas and Bartosikova, 2013; Rhein-Knudsen 2015; Cunha and Grenha, 2016). *Kappa* carrageenan possesses a strong gelling property, which is reversibly liquefied depending on the temperature, and is one of the valuable materials required for dairy and other products (Distantina et al. 2011). The

molecular structure of carrageenan is at high temperature akin to a random coil, but at a low temperature adopts a helical structure while in the presence of potassium at the low temperature, it will form aggregation of helices (fig. 2) (Rhein-Knudsen et al., 2015).

Advantages of carrageenan

Carrageenan has many useful properties in several biological and industrial applications. Carrageenan plays important biological roles in immunomodulatory, anticoagulant, antithrombotic, antiviral, and antitumor responses (Necas and Bartosikova, 2013). Carrageenan has been used for anti-inflammatory in rat paw edema (Sugishita et al. 1981; Henriques et al. 1987; Jain et al. 2001; Paschapur et al. 2009; Petersson et al. 2001; Sini et al. 2010). Carrageenan is a sulfated polysaccharide with the ability to function as an anticoagulant due to the sulfate content (Shanmugam and Mody, 2000). Furthermore, Carrageenan was also reported to be a selective inhibitor of several enveloped viruses, including human pathogens, such as human immunodeficiency virus (HIV), herpes simplex virus (HSV), human cytomegalovirus, human rhinoviruses, and others (Girond et al. 1991; Marchetti et al. 1995; Carlucci et al. 1999; Caceres et al. 2000; Zacharopoulos and Phillips, 1997; Stiles et al. 2008). In the industry, carrageenan has been widely used as a gelling, stabilizing, and thickening additive in food, cosmetics, and industrial pharmacy products. Especially in the food and pharmaceutical industries, carrageenan has been applied for cell immobilization in a fermentation batch reactor (Asanza-Teruel et al. 1997; Nigam, 2000). Finally, carrageenan is used in air freshener gels, toothpaste, firefighting foam, shampoo, cosmetic creams, and shoe polish (Necas and Bartosikova, 2013). Due to all these properties and functions, carrageenan is of high demand in many industries with the annual global market of carrageenan was up to 762.35 million USD in 2013.

Problem in seaweed farming

Since the cost of the production of carrageenan depends on the yield from the algal body, the quality of the seaweed simply refers to the yield of carrageenan, which is usually about 50% in dry weight of the seaweed. The production efficiency and carrageenan distribution in the algal body have not been studied in detail yet. Besides, instability of environmental conditions remains an uncontrollable factor for carrageenan production, i.e., temperature, pH, salinity, and, importantly, disease. The seaweed disease is one of the formidable problems in seaweed plantation. "*Ice–ice*" disease is the most famous seaweed disease caused by a bacterial pathogen. *Ice-ice* disease leads to a characteristic whitening and softening of the infected part of the algal body and causes fragmentation of the plant (Mendoza et al. 2002). Environmental conditions play important roles in the infection of bacterial pathogen in seaweed farming (Case et al. 2011).

Global warming is the most critical environmental issue imposing significant negative effects on aquaculture (Harley et al. 2012). Increasing global concentrations of atmospheric CO_2 making glass house effects that affect increasing seawater temperature and marine acidification (Wootton et al. 2008, Harley 2011). Brown (1995) reported that increasing temperature and salinity suppress the growth of the algal body and carrageenan production in seaweed *Solieria chordalis*. This is due to the alteration in ocean conditions, which leads bacterial infection of the seaweed, especially during mass farming in a plantation. Decreasing seaweed production in the Philippines is due to *ice-ice* disease, as reported by Largo et al. (1995). The *Ice-ice* disease causes loss of the seaweed thallus stimulating cell wall degradation by enzymes produced by bacterial pathogens (Distel et al. 2002; Weiner et al. 2008). Bacteria belonging to the genera *Vibrio, Alteromonas, Cytophaga, Flavobacterium,* and *Pseudoalteromonas* produce enzymes capable of depolymerizing polysaccharides (Goecke et al. 2010). Bacterial interaction on seaweed body was facilitated by bacterial quorum sensing (QS) system such as biofilm formation, bioluminescence,

secondary metabolite production, motility, and virulence functions (Atkinson and Williams, 2009). On the other hand, many studies have reported that seaweed produces QS inhibitors to interrupt communication circuit in bacteria resulting inhibition of gene expression and colonization phenotype (Gonzalez and Keshavan, 2006). The ability to overcome bacterial pathogen interference, macroalgae produce QS inhibitor such as: hypobromus acid produced by brown macrolaga that able to interferes with QS regulated gene expression by deactivating acylated homoserine-lactone (AHL) signal; halogenate furanones from red macroalga *Delisea pulchra*, which act as AHL signal and inhibit gene expression; betocinine, floridoside and isethionic acid produced by *Ahnfeltiopsis flabeliformis*, which can modulate gene expression by competing AHL signal (Egan et al. 2014)

Study of seaweed with vibrational spectroscopy

A rapid and effective analytical tool is necessary to study the process occurring during bacterial invasion into the algal body in order to control bacterial infection on seaweed. The problems and the current situation in this research field motivated me to apply vibrational spectroscopy to investigate enzymatic reaction in seaweed body. Vibrational spectroscopy has a several advantages, such as being non-destructive, environmental friendly, requiring minimal or no sample preparation, and short period of time measurement (Teixeira dos Santos et al. 2016). Vibrational spectroscopy observes interactions between the vibrational motions of a molecule and photons irradiated towards the molecule. The vibrational modes of the molecule is observed by infrared (IR), near-infrared (NIR) and Raman spectroscopies (Ferraro et al. 2003). IR spectroscopy is a form of absorption spectroscopy, which follows the Beer-Lambert law. In contrast, Raman spectroscopy measures scattered light energy, which does not follow the law (Ferraro et al. 2003). Seaweed and carrageenan has been extensively studied using vibrational spectroscopy. For

example, infrared spectroscopy was applied for characterizing carrageenan in 1968 by Anderson et al. while Raman spectroscopy was utilized for the same task 20 years later by Malfait et al. in 1987. The studies were made on extracted and purified carrageenan molecules. IR and Raman spectroscopies were applied for the characterization of chemical contents in several types of dried and grounded seaweed by Pereira et al. (2009, 2011, and 2013) and Rodrigues et al. (2015). Of particular interest is that de Vega et al. (2017) studied the distribution of carrageenan in fresh algal body by fluorescent microscopy by labeling carrageenan with fluorochrome. However, this labeling method is difficult to apply to the quantitative analysis of bacterial degradation of carrageenan, because it is quite difficult to make perfectly homogeneous staining of the pigment of the inhomogeneous algal body.

The limitation of vibrational spectroscopy for plant sample

The application of IR and Raman spectroscopies has some limitations for fresh plant materials (Gierlinger and Schwanninger, 2007). IR and NIR spectra have a strong interference from water as water has strong absorption bands all over the spectral area due to its large dipole moment. In contrast, Raman spectroscopy has low interference of water in the sample, which gives a large advantage in its application of characterizing biological samples. The major disadvantage of Raman spectroscopy is the inherent fluorescence of photosynthetic pigments, such as chlorophyll and carotenoids, existing in the plant body. Chlorophyll and carotenoid are usually abundant in plant samples and are part of the light-harvesting proteins of photosynthetic organisms (Kish et al. 2016). Their fluorescence is often observed in the Raman spectra, when the energy of excitation light is greater than the transition energy between the lowest electronic levels. The scattering cross-section of Raman scattered light is less than 10^{-7}, which is smaller by 5 to 6 orders of magnitude than that of fluorescence.

A resonance enhancement effect is another issue created by the presence of the photosynthetic pigments. The resonance effect is often observed when the wavelength of excitation laser is within or close to the electronic absorption band. The order of the enhancement is up to 10^3-10^5 (Ferraro et al, 2003). The strong resonant bands can overwhelm the bands of interest, in this case the plant body materials. The resonance Raman effect was widely used to study natural pigments (Sato et al. 1995a, 1995b; Ruban et al. 1995; Kish et al. 2016). The natural pigments of biological samples were studied using several different excitation lasers, for example 488 nm for carotenoid, 441.6 nm for chlorophyll *a* and *b*, and 413.1 nm for chlorophyll *a* and carotenoid (Ruban et al. 1995).

The fluorescence effect is often observed when a visible laser is used, but a NIR light is able to reduce the fluorescence effect. An application of 1064 nm laser combined with a Fourier-transform spectrometer allowed the avoidance of fluorescent interference. The technique was referred to as near infrared Fourier Transform (NIR-FT) Raman spectroscopy and applied to plant samples (Hirschfeld Chase, 1986; Sato et al. 1995a; 1995b). Use of NIR-FT Raman spectroscopy has several disadvantages, i.e., lowering in spatial resolution, low sensitivity, and thermal emission effect (Schrader et al. 1991). In the present study, Raman spectroscopy imaging combining with chemometrics analysis was used to investigate enzymatic polysaccharide degradation activity in the algal body in spite of the challenge of the fluorescence effect from such samples.

Chemometric Analysis

Chemometrics is aimed at extracting relevant chemical information out of the measurements by employing various statistical algorithms to all types of analytical data. However, Raman spectroscopy is rarely applied for quantitative analysis because it is quite difficult to obtain the absolute intensity of a signal. Unlike IR and NIR spectroscopies, the spectral intensity of a

Raman spectrum depends on many factors, such as laser power, focal distance from the sampling point, and optical throughput of the Raman spectrometer. IR and NIR spectroscopies are forms of absorption spectroscopy in which the Beer-Lambert law is applied for the quantitative analysis. Chemometric analysis in Raman spectra is achieved by so-called spectral processing. Processing of spectra normally consists of minor manipulation, such as smoothing, averaging, mean centering, baseline removal, zeroing baseline, and normalization (Ferraro et al, 2003). However, in the case of imaging Raman spectroscopy that produces about 10.000 to 100.000 spectra within one sample, this seems difficult to analyze. In this study, I have employed and improved several spectral processing techniques to overcome this problem. New spectral processing software has been developed for interpolation, background subtraction, baseline correction, and internal standard normalization with MatLab R2007b (The Mathwork, Inc, US). The interpolation process increases number of sampling points by adding artificially calculated data using polynomial fitting. The background subtraction removes unnecessary spectral interferences due to water, glass dish, stray lights, and so on, from the raw data. As mentioned previously, auto-fluorescence often observed from natural pigment in biological samples. To remove interference due to the baseline undulations by the auto-fluorescence, dark current of the charge-coupled device (CCD) detector, and other instrumental noise, a sixth order polynomial curve fitting method is applied. In order to compare spectral intensity from one sample to another, internal standard normalization is applied. In absorption spectroscopy, many normalization techniques have been reported, including vector normalization, min-max normalization, and multiplicative scatter correction (Bag et al. 2011). Unfortunately, it is impossible to apply most of those techniques because the Beer-Lambert law is not applicable to emission spectroscopy methods, such as Raman spectroscopy. I have applied a normalization technique using a single major sharing band, which is due to a well-known material

in the sample as a standard. Therefore, the quantitative analysis in the present research is semi-quantitative analysis in which the concentration of the target material is relative to the material that corresponds to the standard band.

Partial Least Square Regression (PLSR) analysis is a qualitative technique often used in the present study, as it is more robust than other least square methods, such as classical least square (CLS) analysis. The PLSR analysis requires a number of test samples to create a calibration curve, but it is stable against perturbations and noise in Raman data and therefore especially suitable for data obtained from biological samples. The PLSR analysis is a technique used to obtain the most suitable calibration model to fit both the X- and Y-matrices simultaneously by selecting latent (or hidden) variables in X, which gives best prediction of the latent variables in Y (Wold et al. 2001). The model were made from the most significant component extracted from all data set of Raman spectra. Cross Validation were employed to test the predictive significance and determine the number of components (Wold et al. 2001). Unlike the CLS method that requires full knowledge of all components in the test samples of the measured system, the PLSR method can work with only knowledge of the substance or material of interest (Nadler and Ronald, 2005). On the other hand, to make a robust quantitative analysis using PLSR method, a huge number of test samples are required to build PLSR model due to a complex multicomponent system in the sample (Nadler and Ronald, 2005).

Synopsis of the work described in each chapter of the thesis

This study consists of three chapters. The aim of this research was to develop a new analytical technique to improve aquaculture production. In the chapter 1, I will demonstrate a robust and low cost quantitative analysis to monitor a starch degrading enzyme reaction. Decreasing the number of PLSR model is my strategy to lower the cost of the analytical technique.

Using PLSR is usually regarded as an irregular procedure, as it may reduce the reliability of the quantitative model. I have found that the selection of the band area in the Raman spectra is able to improve the prediction model, because of its increasing specificity even with a small number of the test samples.

Amylase enzymes are used in this study because of their simple enzymatic functions. Amylase hydrolyzes the common amylose into small sugars, such as maltose and glucose. Enzymatic components in amylase system (starch, maltose and glucose) have simple Raman spectra. The selected enzymatic system is my strategy to study the activity in the algal body, because, Raman spectra of seaweed *K. alvarezii* also consists of relatively simple components. The ability of Raman spectroscopy to analyze the speed of enzymatic reactions in a cell-sized volume is discussed.

In chapter 2, the morphology and carrageenan distribution of *K. alvarezii* was studied with 3 dimensional (3D) Raman image technique to obtain basic knowledge of carrageenan production in the algal body. Good quality *K. alvarezii* contains about 40-50% of carrageenan in dried weight. Imaging Raman spectroscopy combined with PLSR analysis was employed to predict the concentration of carrageenan in algal body. The PLSR model was built using only 11 test samples following my previous study (chapter 1). The hyperspectral images consist of a number of Raman spectra that was measured at several thousand sampling points in the sample. The sampling points were aligned with several 50 to 250 μm intervals in the X-, Y-, and Z-axis in the measured area. I demonstrate the potential of the 3D Raman image in the investigation of distribution and concentration of carrageenan in the algal body. The issue of fluorescence interference is overcome by reducing the naturally occurring pigments by photo-degradation during the sun-drying

procedure of the seaweed. The concentrations of rich and poor carrageenan branches of *K. alvarezii* were described in this chapter.

In chapter 3, the techniques developed in chapters 1 and 2 were evaluated with practical samples. The enzymatic activity was studied in seaweed body during the decomposition due to microorganisms. I searched a naturally decomposed *K. alvarezii* sample to collect bacteria having an enzyme to decompose carrageenan. The bacteria were selected by culturing in a low nutrient environment with carrageenan as the sole source of carbon to find bacteria producing a crude external enzyme. The degradation process of the algal body by the bacteria was then studied with the developed techniques, in which decomposition of carrageenan was quantitatively investigated in order to estimate the process of bacterial invasion and decomposition the algal body.

References

Anderson WS, Dolan TCS, Penman A, Rees DA, Muller GP, Stancioff GP, Stanley NF (1968) Carrageenans. Part IV. Variations in the structure and gel properties of κ-carrageenan, and the characterization of sulphate esters by infrared spectroscopy. J Chem Soc C: 602-606.

Asanza-Teruel ML, Gontier E, Bienaime C, Nava-Saucedo JE, Barbotin JN (1997) Response surface analysis of chlortetracycline and tetracycline production with κ-carrageenan immobilized Streptomyces aureofaciens. Enzyme Microb Technol 21: 314–320.

Ask EI, Batibasaga A, Zertuche-González JA, San M de (2003) Three decades *of Kappaphycus alvarezii* (Rhodophyta) introduction to non-endemic locations. Proceedings of the 17th International Seaweed Symposium, South Africa, pp 49-57.

Atkinson S, and Williams P (2009) Quorum sensing and social networking in the microbial world. J R Soc Interface 6: 959–978.

Bag SK, Srivastav PP, Mishra HN (2011) FT-NIR Spectroscopy: A Rapid Method for Estimation of Moisture Content in Bael Pulp. Brit Food J 113(4): 494-504.

Brown MT (1995) Interactions between environmental variables on growth-rate and carrageenan content of Solieria chordalis (Solieriaceae, Rhodophyceae) in culture. J Appl Phycol 7: 427-432.

Caceres PJ, Carlucci MJ, Damonte EB, Matsuhiro B, Zuniga EA (2000) Carrageenans from chilean samples of *Stenogramme interrupta* (Phyllophoraceae): structural analysis and biological activity. Phytochem 53: 81–86.

Campo VL, Kawano DF, da Silva Jr DB, Carvalho I (2009) Carrageenans: Biological properties, chemical modifications and structural analysis– A review. Carbohydr Polym 77:167–180.

Carlucci MJ, Scolaro LA, Damonte EB (1999) Inhibitory action of natural carrageenans on *Herpes simplex* virus infection of mouse astrocytes. Chemother 45: 429–436.

Cunha L, Grenha A (2016) Sulfated seaweed polysaccharides as multifunctional materials in drug delivery applications. Mar Drugs 14:42.

de Vega GB, Ceballos JA, Anzalone A, Digman MA, Gratton E (2017) A laser-scanning confocal microscopy study of carrageenan in red algae from seaweed farms near the Caribbean entrance of the Panama Canal. J Appl Phycol 29:495–508.

Distantina P, Wiratni, Fahrurrozi M, Rochmadi (2011) Carrageenan Properties Extracted from *Eucheuma cottonii*, Indonesia. Int J Chem Mol Eng 5:6.

Distel DL, Morrill W, MacLaren-Toussaint N, Franks D, Waterbury J (2002) Teredinibacter turnerae gen. nov., sp. nov., a dinitrogen-fixing, cellulolytic, endosymbiotic gamma-proteobacterium isolated from the gills of wood boring molluscs (Bivalvia: Teredinidae). Int J Syst Evol Microbiol 52: 2261–69.

Egan S, Fernandes ND, Kumar V, Gardiner M, Thomas T (2014) Bacterial pathogens, virulence mechanism and host defense in marine macroalgae – minireview. Environ Microbiol 16(4): 925–938.

Egan S, Harder T, Burke C, Steinberg P, Kjelleberg S, Thomas T (2013) The seaweed holobiont: understanding seaweed-bacteria interactions. FEMS Microbiol Rev 37: 462–476.

Egan S, Fernandes ND, Kumar V, Gardiner M, Thomas T (2014) Bacterial pathogen, virulence, mechanism and host defence in marine macroalgae. Environ Mibrobiol 16 (4): 925-938.

Ferraro JR, Nakamoto K, Brown CW (2003) Introduction Raman Spectroscopy. Academic Press, New York.

Gierlinger N, Schwanninger M (2007) The potential of Raman microscopy and Raman imaging in plant research. Spec 21: 69–89.

Girond S, Crance JM, Van Cuyck-Gandre H, Renaudet J, Deloince R (1991) Antiviral activity of carrageenan on hepatitis A virus replication in cell culture. Res Virol 142: 261–270.

Goecke F, Labes A, Wiese J, Imhoff J (2010) Chemical interactions between marine macroalgae and bacteria. Mar Ecol Prog Ser 409: 267–299.

Gonzalez JE, Keshavan ND (2006) Messing with bacterial quorum sensing. Microbiol Mol Biol Rev 70: 859-875.

Harley CDG (2011) Climate change, keystone predation, and biodiversity loss. Sci 334:1124–7.

Harley CDG, Anderson KM, Demes KW, Jorve JP, Kordas RL, Coyle TA, Effects of climate change on global seaweed communities. J Phycol 48: 1064–1078.

Henriques MGMO, Silva PMR, Martins MA, Flores CA, Cunha FQ, Assreuy-Filho J, Cordeiro RSB (1987) Mouse paw oedema. A new model for inflammation? Braz J Med Biol Res 20: 243–249.

Hirschfeld T, Chase B (1986) FT-Raman spectroscopy: development and justification. Appl Spec 40(2): 133 – 137.

Jain NK, Patil CS, Singh A, Kulkarni SK (2001) A simple technique to evaluate inflammatory pain along with anti-inflammatory studies in carrageenan-induced paw edema. Indian J Pharmacol 33: 114–115.

Karsten U, Bischof K, Wiencke C (2001) Photosynthetic performance of Arctic macroalgae after transplantation from deep to shallow waters. Oecologia 127: 11–20.

Kish E, Wang K, Llansola-Portoles MJ, Ilioaia C, Pascal AA, Robert B, Yang C (2016) Probing the pigment binding sites in LHCII with resonance Raman spectroscopy: The effect of mutations at S123. Biochim Biophys Acta 1875: 1490–1496.

Largo DB, Fukami K, Nishijima T, Ohno M (1995) Laboratory-induced development of the ice-ice disease of the farmed red algae *Kappaphycus alvarezii* and *Eucheuma denticulatum* (Solieriaceae, Gigartinales, Rhodophyta). J Appl Phycol 7: 539-543.

Lechat H, Amat H, Mazoyer J, Gallant DJ, Buléon A, Lahaye M (1997) Cell wall composition of the carrageenophyte *Kappaphycus alvarezii* (Gigartinales, Rhodophyta) partitioned by wet sieving. J Appl Phycol 9:565–572.

Malfait T, Van Dael H, Van Cauwelaert F (1987) Raman spectroscopic analysis of the sodium salt of kappa-carrageenan and related compounds in solution. Carbohydr Res 163: 9–14.

Manuhara GJ, Praseptiangga D, Riyanto RA (2016) Extraction and characterization of refined κ-carrageenan of red algae [*Kappaphycus alvarezii* (Doty ex P.C. Silva, 1996)] originated from Karimun Jawa Islands. Aquat Procedia 7:106 – 111.

Marchetti M, Pisani S, Pietropaolo V, Seganti L, Nicoletti R, Orsi N (1995): Inhibition of *Herpes simplex* virus infection by negatively charged and neutral carbohydrate polymers. J Chemother 7: 90–96.

Mendoza WG, Montaño NE, Ganzon-Fortes ET, Villanueva RD (2002) Chemical and gelling profile of ice-ice infected carrageenan from *Kappaphycus striatum* (Schmitz) Doty "sacol" strain (Solieriaceae, Gigartinales, Rhodophyta). J Appl Phycol 14: 409.

Nadler B, Coifman RR (2005) The prediction error in CLS and PLS: the importance of feature selection prior to multivariate calibration. J Chemom 19:107–118.

Necas J, Bartosikova L (2013) Carrageenan: A review. Vet Med 58(4):187–205.

Normah O, Nazarifah I (2003) Production of semi-refined carrageenan from locally available red seaweed, *Eucheuma cottonii* on a laboratory scale. J Trop Agric and Fd Sc 31(2):207–213.

Paschapur MS, Patil MB, Kumar R, Patil SR (2009) Evaluation of anti-inflammatory activity of ethanolic extract of *Borassus flabellifer* L. male flowers (inflorescences) in experimental animals. J Med Plants Res 2: 49–54.

Pereira L, Amado AM, Critchley AT, van de Velde F, Ribeiro-Claro PJA (2009) Identification of selected seaweed polysaccharides (phycocolloids) by vibrational spectroscopy (FTIR-ATR and FT-Raman). Food Hydrocoll 30:1-7.

Pereira L, Gheda SF, Ribeiro-Claro PJA (2013) Analysis by vibrational spectroscopy of seaweed polysaccharides with potential use in food, pharmaceutical, and cosmetic industries. Int J Carbohydr Chem 2013: 7p.

Pereira L, Sousa A, Coelho H, Amado AM, Ribeiro-Claro PJA (2003) Use of FTIR, FT-Raman and 13C-NMR spectroscopy for identification of some seaweed phycocolloids. Biomol Eng 20:223-228.

Potin P, Richard C, Barbeyron T, Henrissat B, Gey C, Petillot Y, Forest E, Dideberg O, Rochas C, Kloareg B (1995) Processing and hydrolytic mechanism of the cgkA-encoded κ-carrageenase of *Alteromonas carrageenovora*. Eur J Biochem 228: 971–975.

Rhein-Knudsen N, Ale MT, Meyer AS (2015) Seaweed hydrocolloid production: An update on enzyme assisted extraction and modification technologies. Mar Drugs 13:3340-3359.

Rodrigues D, Sousa S, Silva A, Amorim M, Pereira L, Rocha-Santos TA, Gomes AM, Duarte AC, Freitas AC (2015) Impact of enzyme- and ultrasound-assisted extraction methods on biological properties of red, brown, and green seaweeds from the central west coast of Portugal. J Agric Food Chem 63(12): 3177-3188.

Ruban AV, Horton P, Robert B (1995) Resonance Raman spectroscopy of the photosystem i1 light-harvesting complex of green plants: a comparison of trimeric and aggregated states. Biochem 34: 2333-2337.

Sato H, Okada K, Ueharaan K, Ozaki Y (1995a) Near-Infrared Fourier-Transform Raman study of chlorophyll *a* in solutions. Photochem Photobiol 61(2): 175-182.

Sato H, Uehara K, Ishii T, Ozaki Y (1995b) FT-IR and Near-Infrared FT-Raman study of aggregation of bacteriochlorophyll *c* in solutions: evidence for involvement of the ester group in the aggregation. Biochem 34: 7854-7860.

Schrader B, Hoffmann A, Simon A Sawatzki J (1991) Can a Raman renaissance be expected via the near-Infrared Fourier-Transform technique. Vib Spectrosc 1(3): 239–250.

Shanmugam M, Mody KH (2000) Heparinoid-active sulphated polysaccharides from marine algae as potential blood anticoagulant agents. Curr Sci 79: 1672–1683.

Sini JM, Yaro AH, Ayanwuyi LO, Aiyelero OM, Mallum SM, Gamaniel KS (2010) Antinociceptive and anti-inflammatory activities of the aqueous extract of the root bark of Combretumsericeum in rodents. Afr J Biotechnol 9: 8872–76.

Soegiarto A, Sulustijo (1990) Utilization and farming of seaweeds in Indonesia. In Dogma IJ Jr, Trono GC Jr, Tabbada RA (Ed) Culture and use of algae in southeast Asia, Proceedings of the Symposium on Culture and Utilization of Algae in Southeast Asia, 8-11 December 1981, Philippines, pp 9-19

Stiles J, Guptill-Yoran L, Moore GE, Pogranichniy RM (2008) Effects of κ-carrageenan on in vitro replication of feline herpesvirus and on experimentally induced herpetic conjunctivitis in cats. Invest Ophthalmol Vis Sci 49: 1496–1501.

Sugishita E, Amagaya S, Ogihara Y (1981) Anti-inflammatory testing methods: comparative evaluation of mice and rats. J Pharmacobio-Dyn 8: 565–575.

Teixeira dos Santos CA, Páscoa RNMJ, Lopes JA (2017) A review on the application of vibrational spectroscopy in the wine industry: from soil to bottle. Trend Anal Chem 88:100-108.

Toohey BD, Kendrick GA (2007) Survival of juvenile *Ecklonia radiata* sporophytes after canopy loss. J Exp Mar Biol Ecol 349: 170–182.

Wahl M, Goecke F, Labes A, Dobretsov S, Weinberger F (2012) The second skin: ecological role of epibiotic biofilms on marine organisms. Front Microbiol 3: 292.

Weiner RM, Taylor LE, Henrissat B, Hauser L, Land M, Coutinho PM, et al. (2008) Complete genome sequence of the complex carbohydrate-degrading marine bacterium, *Saccharophagus degradans* strain 2-40T. PLoS Genet 4: e1000087.

Wold S, Sjöström M, Eriksson L (2001) PLS-regression: a basic tool of chemometrics. Chemometr Intell Lab Syst 58: 109-130.

Wootton JT, Pfister CA, Forester JD (2008) Dynamic patterns and ecological impacts of declining ocean pH in a high-resolution multi-year dataset. Proc Nat Acad Sci 105:18848–53.

Zacharopoulos VR, Phillips DM (1997) Vaginal formulations of carrageenan protect mice from *Herpes simplex* virus infection. Clin Diagn Lab Immunol 4: 465–468.

Figures

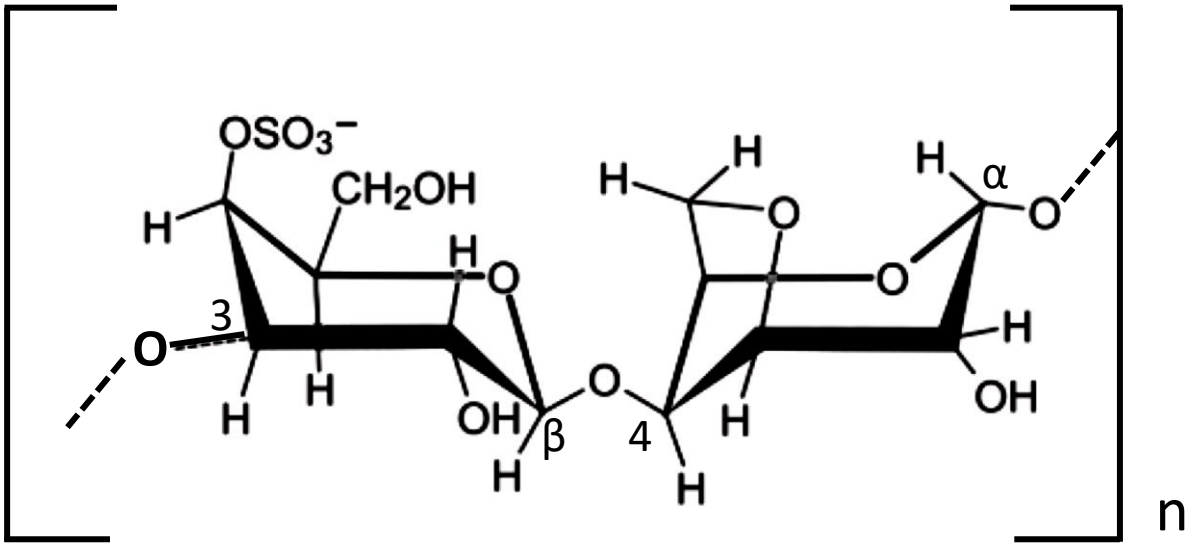

Fig 1. Chemical structure of monomer unit in kappa (κ)-carrageenan.

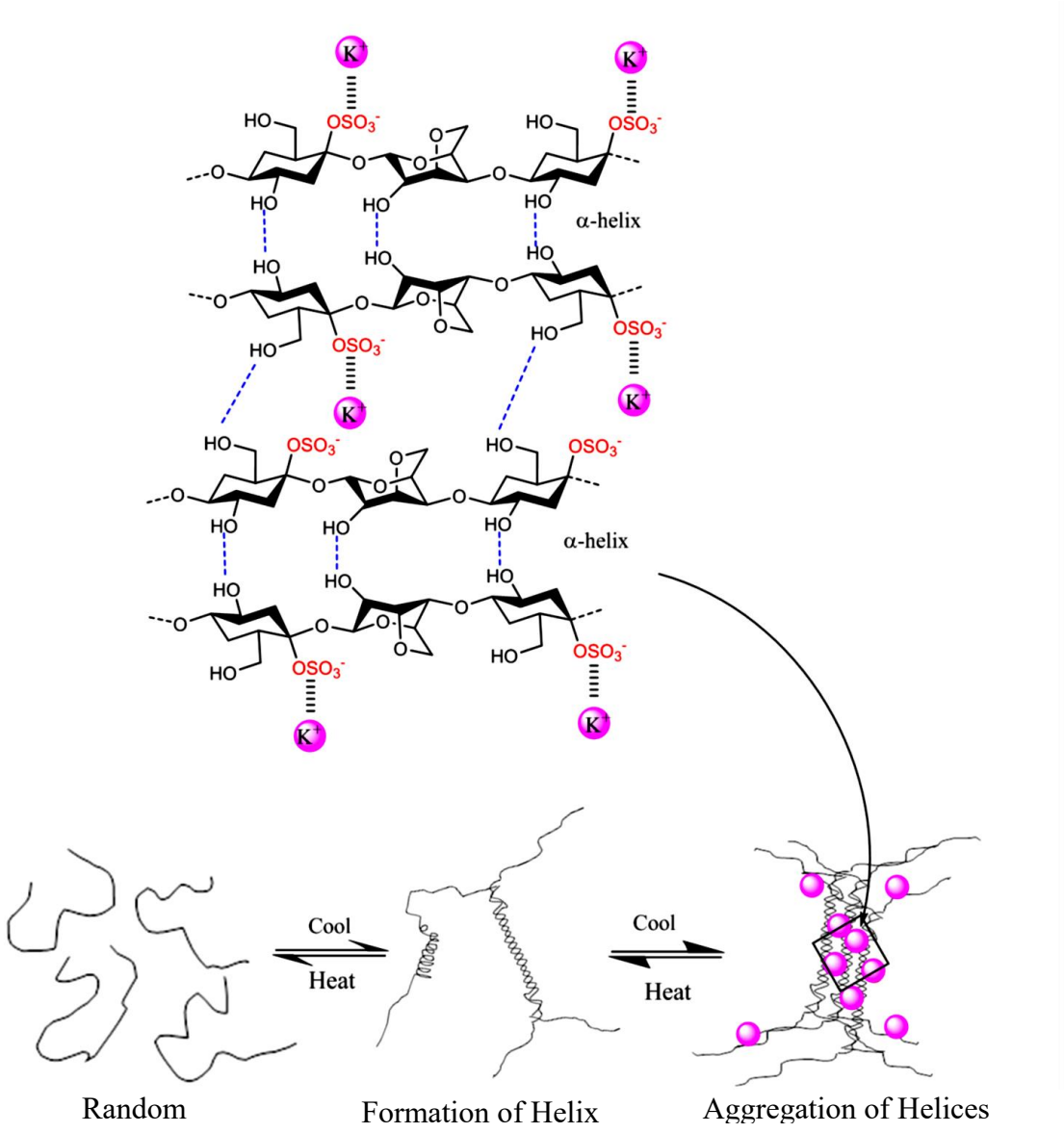

Fig 2. Phase transition of κ-carrageenan into three gel structures (Rhein-Knudsen et al. 2015).

Chapter 1

Development of Quantitative Analysis Techniques for Saccharification Reactions Using Raman Spectroscopy

Abstract

A low cost and robust quantitative analysis to quantify each enzymatic component using Raman spectroscopy were describe in this study. It is a micro-volume, quantitative, and in situ technique, which can be used for studying saccharification processes in plant tissues. Prediction models for quantitative analysis of maltose, glucose, and starch were built with partial least square regression (PLSR) analysis to monitor the saccharification process caused by α-amylase. We examined the reliability of the prediction models built with a small number of test samples, only 7 samples. The spectral regions used to build the models were optimized for each sugar and were selected in such a manner that they did not overlap with strong protein and lipid bands that generally exist in plant tissues. The models were validated by monitoring the composition of reducing sugars and starch in a reactor and comparing the results with those obtained by a conventional method. The results of Raman analysis and the conventional method showed good agreement for the reaction with α-amylase; however, it is not perfect for reactions with a different enzyme, especially β-amylase. The results suggest that the present Raman technique is reliable and useful for sugar analysis; however, the prediction model built for a specific enzyme is valid only for that enzyme.

Keywords

Sugar, Raman spectroscopy, Quantitative analysis, Chemometrics, Plant analysis

Introduction

Sugar production through enzymatic reactions comprises a large sector of the food and beverage industries worldwide (Sugar and Bour, 2016). Generally, source of sugar production by enzymatic reaction is polysaccharide of biomass (Binder and Raines, 2010). The process of hydrolytic degradation for polysaccharides into simple sugar is referred to as saccharification. The main sugar components can be categorized as sucrose, glucose, fructose, and maltose. Sugar composition is essential for many physical properties, such as hygroscopic affinity, granulation, viscosity, and energy value (Ouchemoukh et al. 2010). However, independent determination of glucose and maltose in sugar is difficult when conventional methods are used. Nearly 40%–90% of maltose found in maltose syrups is purified starch hydrolysate (Gaouar et al. 1998). Pure maltose has been employed in the manufacture of vaccines, food, maltitol, antibiotics, etc., for which crystallized maltose purified from syrups is often used (Okada and Nakakuki, 1992). Studies on corn and rice for starch production have already been conducted by several researchers. Maize (corn) kernels are a major raw material for sugar and chemical production, with starch providing up to 70%–74% of the kernel weight (Shobha et al. 2010). Rice, a staple food of Asian countries, contains up to almost 80% starch (Mohan et al. 2005). The main enzymes used in the industry are amylases that hydrolyze the 1,4-glycosidic bond. Amylases converts starch molecules into smaller oligosaccharides and glucose. The major sources of α-amylases are plants, animals, microorganisms, and algae (de Souza and Magalhaes, 2010). Hence, it is necessary to analyze the saccharification process quantitatively in biomasss, to investigate the effective saccharification process, especially localized enzymatic reaction in cellular level.

Raman spectroscopy is one of the most promising noninvasive methods for observing the distribution of carrageenan in situ. It is a sensitive and reliable tool for determining biochemical

changes in biological samples, with no need for any labeling or chemical purification processes. In addition, the applications of Raman spectroscopy can be expanded with other techniques, such as Raman imaging and remote measurement with Raman probes (Katagiri et al. 2009; Komachi et al. 2005; Hattori et al. 2007). In this study, we aimed to develop a technique for quantitative analysis of localized saccharides produced by a specific enzyme, which requires small sample volumes based on Raman spectroscopy using multivariate analysis. The capability and accuracy of the technique were evaluated and discussed. Although the main target of the analysis was reaction with α-amylase, the feasibility of the analytical model to β-amylase was also examined. With conventional methods that analyze reducing sugars, it is difficult to measure glucose and maltose independently (Tihomirova et al. 2016). High-performance liquid chromatography (HPLC) is often used for the quantitative analysis of specific saccharides (Meyer et al. 2001; Xi et al. 2016; Ai et al. 2016). Özbalci et al. (2013) revealed that Raman spectroscopy can be used to quantify glucose, fructose, sucrose, and maltose contents independently in honey samples. Hence, Raman spectroscopy has high viability for the present purpose, i.e., for nondestructive, real-time, micro-volume, and quantitative analysis, which would be reliable for sugar analysis. PLSR analysis was employed for the purpose, because it is more robust than other least square methods, such as classical least square (CLS) analysis, to perturbations and noise. However, PLSR analysis requires building a robust prediction model for targeted material. For conducting saccharification of starch into glucose and maltose, independent prediction models are required for each targeted sugar. Moreover, collinearity of the materials must be avoided in the test samples to build the prediction model. To analyze glucose, maltose, and starch independently, an extremely large number of test samples is required. Hence, we have attempted to reduce the number of test sample in the present study, because we are considering a specific enzyme. The enzyme always has its

specific reaction pattern, the model could be much simpler. In the present study, we have examined the feasibility of a simple PLSR model built with a small number of test samples in the empirical condition with Raman spectra, which have strong noise and perturbation, such as baseline undulation due to fluorescence and white noise due to weak Raman scattered light.

Materials and methods

Enzyme assay

Alpha-amylase (EC 3.2.1.1) enzyme from *Aspergillus oryzae* and β-amylase (EC 3.2.1.2, Sigma–Aldrich) were purchased. Fresh soluble starch, D-glucose, and maltose (Wako Pure Chem. Ind. Ltd., Japan) were also purchased and used without further purification. The enzymatic reaction of α-amylase was conducted at room temperature, while β-amylase was reacted at 20°C. The α and β-amylase activity were estimated based on the amount of reducing sugar produced from starch by using the Miller method.[17] Soluble starch (10,000 mg/L) in phosphate buffer (pH 7.0) was preheated at 60°C for 5 min before adding 150 unit/mg α-amylase or β-amylase. The reaction mixture was incubated for 2 h, and the samples were taken at 0, 1, 3, 5, 10, 15, 30, 45, 60, 90, and 120 min from the reaction container. A small portion picked up during the reaction was immediately mixed with dinitrosalicylic acid (DNSA) and boiled at 100°C for 10 min following Miller's (1959) procedure. The samples were then transferred to a UV spectrometer to measure absorption at 540 nm to quantify the sugar production. The other portion picked up for the Raman measurement was boiled for only 5 min to denature the enzyme.

Preparation of model mixtures

Model mixtures for estimating the enzymatic component (starch, D-glucose, and maltose) were obtained by mixing several concentrations of starch (0–10,000 mg/L) and sugars (D-glucose

or maltose; 0–8,000 mg/L) in phosphate buffer (pH 7.0). The concentrations of these materials in the model series are listed in Table 1. Aliquots (5 μL) from models and enzymatic reactions were dropped onto a quartz bottomed disk (27 mm in diameter) and dried by using a vacuum desiccator for 5 min. Samples were then analyzed by Raman spectroscopy.

Raman measurement

The Raman measurement of the samples was carried out by using a homemade confocal Raman system. The system was equipped with an inverted microscope (IX73, Olympus, Japan), a polychromator (Grating: 600 l/mm, 750 nm-blazed, f = 320 mm, Photon Design Co., Japan), a cooled CCD detector (DU401-BR-DD, Andor Technology), and a diode laser (785 nm, Toptica, Germany). A water-immersed objective lens (×60, NA 1.2; Olympus, Tokyo, Japan) was used for the measurements. The exposure time was 10 s × 3 times with excitation light, 60 mW at the sample point. Thirty spectra were collected from each sample over a range of 320–1950 cm^{-1}.

Chemometrics analysis

Raw spectra were pretreated for background correction to remove the effect of the quartz window. To remove dark noise and fluorescence caused by impurities, a sixth-order polynomial baseline correction was employed. The spectra were smoothed by a second-order polynomial (Savitzky–Golay algorithm) with five points on both frequency sides. The spectra were then normalized with a band at 1263 cm^{-1}, which was assigned to the CH_2 bending mode. All spectral processing data was atomized by my own software build in MatLab R2007b (The Mathwork, Inc, US). Partial least square regression (PLSR) analysis was performed by using the Unscrambler 10.1 software (CAMO Software AS., Oslo, Norway).

Result and Discussion

Starch is hydrolyzed into smaller sugars by α-amylase. The enzymatic reaction takes place randomly on starch, a polysaccharide, and produces the oligosaccharides, maltose, and glucose. In this study, a method to monitor this reaction quantitatively was developed using Raman spectroscopy. The purpose in this chapter is to measure the glycation reaction caused by amylase in plant materials; therefore, it is necessary to analyze the reaction per cells size (1-5 μm). The confocal Raman microscope employed in this research was equipped with an object lens with NA 1.2. The highest spatial resolution of this objective lens was estimated to be 0.80 μm. Meanwhile, the spatial resolution estimated from the confocal configuration is 0.98 μm, because the diameter of the confocal pinhole was 65 μm, with a 200-mm focusing lens, and a focusing distance (of the objective lens) of 3 mm. Hence, the diameter of the excitation volume is sufficiently small to observe the reaction in one cell.

Raman spectra of aqueous solutions of phosphate buffer (a), starch (b), D-glucose (c), and maltose (d) are shown in Fig. 1. The spectra of saccharides have few bands in the frequency region higher than 1500 cm^{-1} because they do not have any carbonyl groups or double bonds. Although there is a band near 1640 cm^{-1} due to OH group of saccharides, it is not available for analysis because there is strong overlapping with OH group of water. Söderholm et al. (1999) suggested that the 500–600 cm^{-1} range describes sugar species well. The bands below 600 cm^{-1} can be used to identify these saccharide species, i.e., the bands at 519 cm^{-1} and 554 cm^{-1} in maltose, those at 541 cm^{-1} and 558 cm^{-1} in D-glucose, and a band at 479 cm^{-1} in starch. The band frequencies for maltose and glucose are similar, while their relative intensities are quite different. In the spectrum of the phosphate buffer, a broad band at 1636 cm^{-1} is attributable to the presence of water. Another broad band at 535 cm^{-1} can be attributed to an interaction between phosphate and water, which overlaps the characteristic bands of the saccharides. Lipids and proteins have relatively weak bands

near these band area (Wua et al. 2011). Our final targets are plants with relatively low concentrations of these latter materials; therefore, the bands described are good marker bands for these sugars. Conventional methods that are normally used to analyze reducing sugars struggle to measure glucose and maltose independently. HPLC is often employed to analyze glucose and maltose. It is necessary to prepare a test solution for HPLC that does not include any solid or insoluble materials; therefore, HPLC is not applicable for nondestructive analysis of in situ localized sugars. Hence, Raman spectroscopy has good potential for maltose and glucose analysis as well.

In order to determine the concentrations of maltose and glucose, as well as starch, in the reaction mixture with α-amylase, it is necessary to build reliable calibration curves for Raman analysis. First, a series of test mixtures of starch, D-glucose and maltose in phosphate buffer solution without α-amylase was prepared to build the calibration curve. The concentrations of these materials in the model series can be found in Table 1. The test model has a strong correlation among those sugar concentrations, which is usually an insufficient example for the estimation of each material. Moreover, it lacks oligosaccharides in the model. However, that would not be a problem because an enzyme usually keeps the reaction ratio of its products in a relatively small range. We assumed that the analytical model for maltose or glucose should have a margin in which the target sugar can be independently analyzed when the spectral area to build the model was correctly selected. The Raman spectra of the model solution were very similar to that of the real reaction mixture, i.e., with α-amylase (Fig. 1). There was no band attributable to the amide I mode of α-amylase observed in the spectrum.

Raman spectroscopy is a kind of emission spectroscopy, and hence, the intensity of the spectrum is affected by many instrumental and sample conditions. Therefore, quantitative Raman

analysis without a standard material will be semi quantitative, in which only relative concentrations can be obtained. In the present study, we have used the area of a band near 1263 cm^{-1} attributable to a CH_2 bending mode on the sugar ring, which is minimally affected by the enzymatic reaction. When the initial concentration of starch is known, it is possible to determine the absolute concentrations of glucose and maltose. PLSR calibration models were initially built with spectra of aqueous solutions; however, the Raman bands attributable saccharides were extremely weak to obtain reliable results. The model solutions were then dried up to increase the intensity of the saccharide bands. Hence, the current analysis is semi-quantitative. The model was built for the entire spectral region; however, the result was not perfect because each material exhibited an extremely strong correlation. The model was then recalculated with a reduced spectral region, which was optimized for prediction of maltose, glucose, and starch independently. The best spectral region for maltose and glucose analysis was 500–650 cm^{-1} while it was 460-490 cm^{-1} for starch. The correlation coefficients (R^2) for the model and validation to analyze maltose, glucose and starch were 0.964 and 0.962, 0.927 and 0.923, and 0.900 and 0.890, respectively. Detailed description of the PLSR calibration models is available in the **supplementary information**.

The prediction models were applied to monitor the enzymatic reaction of α-amylase. Figure 2(a) shows the concentration changes of maltose, glucose, and starch analyzed with Raman spectroscopy and that of the reducing sugars (maltose and glucose) analyzed with the Miller method. Soluble starch in phosphate buffer (pH 7.0; 10,000 mg/L) was incubated with α-amylase and its spectrum was acquired after 0, 1, 3, 5, 10, 15, 30, 45, 60, 90, and 120 min. At the same times as the Raman measurements, a portion of the mixture was analyzed by the Miller method (Fig. 2(b)). The concentrations of maltose, glucose, and starch estimated with the PLSR prediction

models are plotted in Fig. 2(a). The concentration of starch reduced quickly in the first minute and reduced slowly after that. In contrast, the concentration of D-glucose, which was the final product, increased quickly in the first minute and continued to increase with time. The concentration of maltose showed a quick increment in the first minute; however, it showed a variation above and below it. The experiments were repeated 20 times, and the results always showed similar tendencies. The concentrations of reducing sugars analyzed by the Miller method is shown in Fig. 2(b). The result of the Miller method showed a similar curve to that of the Raman analysis in the reaction rate, suggesting that the prediction models work correctly in the real α-amylase reaction. The value of sugar concentration drops at 60 min in the graph of the Miller method (Fig. 2(b)), which is not reasonable because α-amylase never causes a reverse reaction. In contrast, the result obtained by Raman analysis (Fig. 2(a)) changes smoothly, which seems to agree with the theory of the enzymatic reaction.

α-Amylase belongs to endoamylase family (Van der Maarel et al. 2002). Endoamylase is able to cut the α-1,4 glycosidic bond in the inner part (endo-) of the amylose or amylopectin chain as well as starch. The main products of this enzyme are maltose, glucose, and oligosaccharides (having more than three D-glucose residue) (Wirnt and Stegbauer, 1974). The ratio of the products is relatively stable, but not exactly the same anytime because the enzymes randomly cut the bonding between saccharides, especially when the reaction is about to achieve the equilibrium point. The present PLSR analytical model was then examined in saccharification processes with different conditions. We employed three conditions: reaction at a lower temperature (10℃), adding excess maltose in the initial state, and using different enzyme (β-amylase). The maltose production curves at 10℃ and 25℃ are compared in Fig. 3. The reaction speed seemed to slightly decrease for the reaction at 10℃ in the first 30 min compared to that at 25℃; however, the concentration

caught up after 120 min of incubation. The reaction speed of the enzyme decreases because of the insufficient temperature; however, the final production depends on the concentration of the initial material (Silva et al. 2010). The result seems to agree with the theoretical results. In the second examination, we evaluated the ability of the present model with a sample that includes one of the final products. The enzymatic reaction does not always start with zero concentration of reducing sugars, in the case where the enzymatic reaction is performed using microorganism (bacteria or fungi), because maltose or glucose is often added into the reaction container to keep their activity. To restage the condition, excess maltose (1,000 mg/L) was added into the starch (10,000 mg/L) to observe the enzymatic reaction of α-amylase. The concentration curves for maltose and glucose estimated by Raman analysis are depicted in Fig. 4(a). The curve of maltose is in excess of 1,000 mg/L larger value relative to that for the sample without excess maltose. In contrast, the value of glucose did not show any difference. The results measured by Miller method is shown in Fig. 4(b). The curve obtained by Miller's method showed unusual reduction in concentration in the curve at 15 min for the sample with additional maltose, which was also observed in the Raman analysis. It suggests that the present Raman-PLSR analysis is robust to this kind of perturbation. The present Raman-PLSR model was examined to monitor the sugar concentration in the reaction with a different enzyme (i.e., β-amylase). β-Amylase belongs to exoamylase, which exclusively cleaves to α-1,4 glycosidic bonds, successively yielding successive of maltose and a few glucose (Pandey et al. 2000) The concentration changes of starch, maltose, and glucose monitored by Raman analysis is depicted in Fig. 5(a). The maltose production by β-amylase was almost twice higher than that of α-amylase, while D-glucose was much lower. The curves suggest that the activity of β-amylase was remarkably high in the first minute, and stabilized thereafter. Because the concentration of the starch was initially 10,000 mg/L, the sum of concentrations of the products

must always be 10,000 mg/L. According to the curves in Fig. 5(a), the sum of the concentration of only maltose and starch is approximately 10,000 mg/L; however, it becomes more than that when the concentration of glucose is added. The concentration change of reducing sugar monitored by Miller's method is depicted in Fig. 5(b). It showed similar concentration to the curve of maltose except for data at 120 min. It is assumed that the prediction value of glucose is a kind of artifact because of incorrect application of the analytical model. The results suggest that the analytical model built for a specific enzyme is valid only for that enzyme.

Conclusion

A confocal Raman microscope with a high NA objective lens realizes high spatial resolution to analyze the reaction in a cell-sized small volume. The PLSR model built with 7 test samples for a specific enzyme is relatively robust to reaction with external perturbation; however, it is not applicable for a different enzyme. Maltose, glucose, and starch were analyzed independently by selecting the spectral area to build the PLSR models, although the test samples exhibit correlations among their concentration values.

References

Ai Y, Yu Z, Chen Y, Zhu X, Ai Z, Liu S, Ni D (2016) Rapid determination of the monosaccharide composition and contents in tea polysaccharides from Yingshuang green tea by pre-column derivatization HPLC. J Chem 2016: 1-5.

Binder JB, Raines RT (2010) Fermentable sugars by chemical hydrolysis of biomass. PNAS 107(10): 4516–4521.

de Souza PM, Magalhaes PO (2010) Application of microbial α–amylase in industry – A review. Braz J Microbiol 41(4): 850-861.

Gaouar 0, Zakhia N, Aymard C, Rios GM (1998) Production of maltose syrup by bioconversion of cassava starch in an ultrafiltration reactor. Ind Crops Prod 7(2-3): 159–167.

Hattori Y, Komachi Y, Asakura T, Shimosegawa T, Kanai G, Tashiro H, Sato H (2007) In vivo Raman study of the living rat esophagus and stomach using a micro raman probe under endoscope. Appl Spectrosc 61(6): 579-584.

Katagiri T, Yamamoto YS, Ozaki Y, Matsuura Y, Sato H (2009) High axial resolution raman probe made of single hollow optical fiber. Appl Spectrosc 63(1): 103-107.

Komachi Y, Sato H, Aizawa K, Tashiro H (2005) Micro optical fiber probe for the use of intravascular Raman endoscope. Appl Opt 44(22): 4722-32.

Meyer A, Raba C, Fischer K (2001) Ion-pair RP-HPLC determination of sugars, amino sugars, and uronic acids after derivatization with p-aminobenzoic acid. Anal Chem 73(11): 2377-82.

Miller GL (1959) Use of dinitrosalicylic acid reagent for determination of reducing sugar. Anal

Chem 31(3): 426–428.

Mohan BH, Gopal A, Malleshi NG, Tharanathan RN (2005) Characteristics of native and enzymatically hydrolyzed ragi (*Eleusine coracana*) and rice (*Oryza sativa*) starches. Carbohydr Polym 59(1): 43–50.

Okada M, Nakakuki T (1992) Oligosaccharides: production, properties and applications. In Schenck FW, Hebeda RE (Ed) Starch hydrolysis products: worldwide technology, production and applications. VCH, New York. Pp. 335–366.

Ouchemoukh S, Schweitzer P, Bey MS, Djoudad-Kadji H, Louaileche H (2010) HPLC sugar profiles of Algerian honeys. Food Chem 121(2): 561–568.

Özbalci B, Boyaci IH, Topcu A, Kadilar C, Tamer U (2013) Rapid analysis of sugars in honey by processing raman spectrum using chemometris methods and artificial neural networks. Food Chem 136(3-4): 1444-52.

Pandey A, Nigam P, Soccol CR, Soccol VT, Singh D, Mohan R (2000) Advances in microbial amylases. Biotechnol Appl Biochem 31(2): 135–152.

Shobha D, Sreeramasetty TA, Puttaramanaik, Pandurange-Gowda KT (2010) Evaluation of maize genotypes for physical and chemical composition at silky and hard stage. J Agric ScI 23(2): 311–314.

Silva RN, Quintino FP, Monteiro VN, Asquieri ER (2010) Production of glucose and fructose syrups from cassava (Manihot Esculenta Crantz) starch using enzymes produced by microorganisms isolated from brazilian cerrado soil. Ciênc Tecnol Aliment 30(1): 213-217.

Söderholm S, Roos YH, Meinander N, Hotokka M (1999) Raman spectra of fructose and glucose

in the amorphous and crystalline states. J Raman Spectrosc 30(11): 1009-18.

Sugar J, Bour P (2016) Quantitative analysis of sugar composition in honey using 532-nm excitation Raman and Raman optical activity spectra. J Raman Spectrosc 47(11): 1298-1303.

Tihomirova K, Dalecka B, Mezule L (2016) Application of conventional HPLC RI technique for sugar analysis in hydrolyzed hay. Agron Res 14(5): 1713–1719.

Van der Maarel MJEC, Van der Veen B, Uitdehaag JCM, Leemhuis H, Dijkhuizen L (2002) Properties and applications of starch-converting enzymes of the α-amylase family. J Biotechnol 94(2): 137-155.

Wirnt R, Stegbauer P (1974) α-Amylase measurement of reducing sugar in Bergmeyer HU (Ed) method of enzymatic analysis. Academic Press Inc, New York and London. 2: 885-890.

Wua H, Volponia JV, Oliverb AE, Parikhb AN, Simmonsa BA, Singh S (2011) In vivo lipidomics using single-cell Raman spectroscopy. PNAS 108(9): 3809–14.

Xi X, Xiao S, Tang F, Chu Q, Lan T, Dong G (2016) Monosaccharide analysis of dendrobium moniliforme polysaccharides by high performance liquid chromatography/electrospray ionization mass spectrometry. Am J Agric For 4(6): 156-162.

Figures

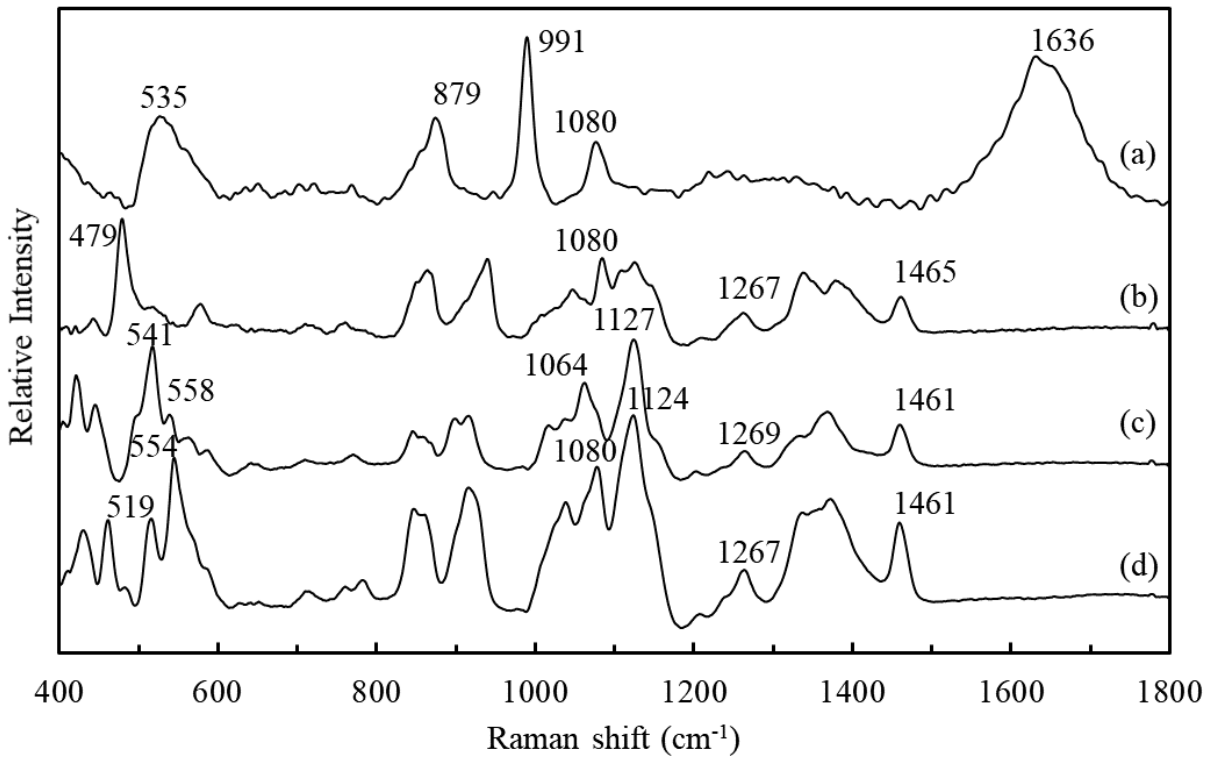

Fig. 1 Raman spectra of phosphate buffer (a), maltose (b), D-glucose (c), and starch (d).

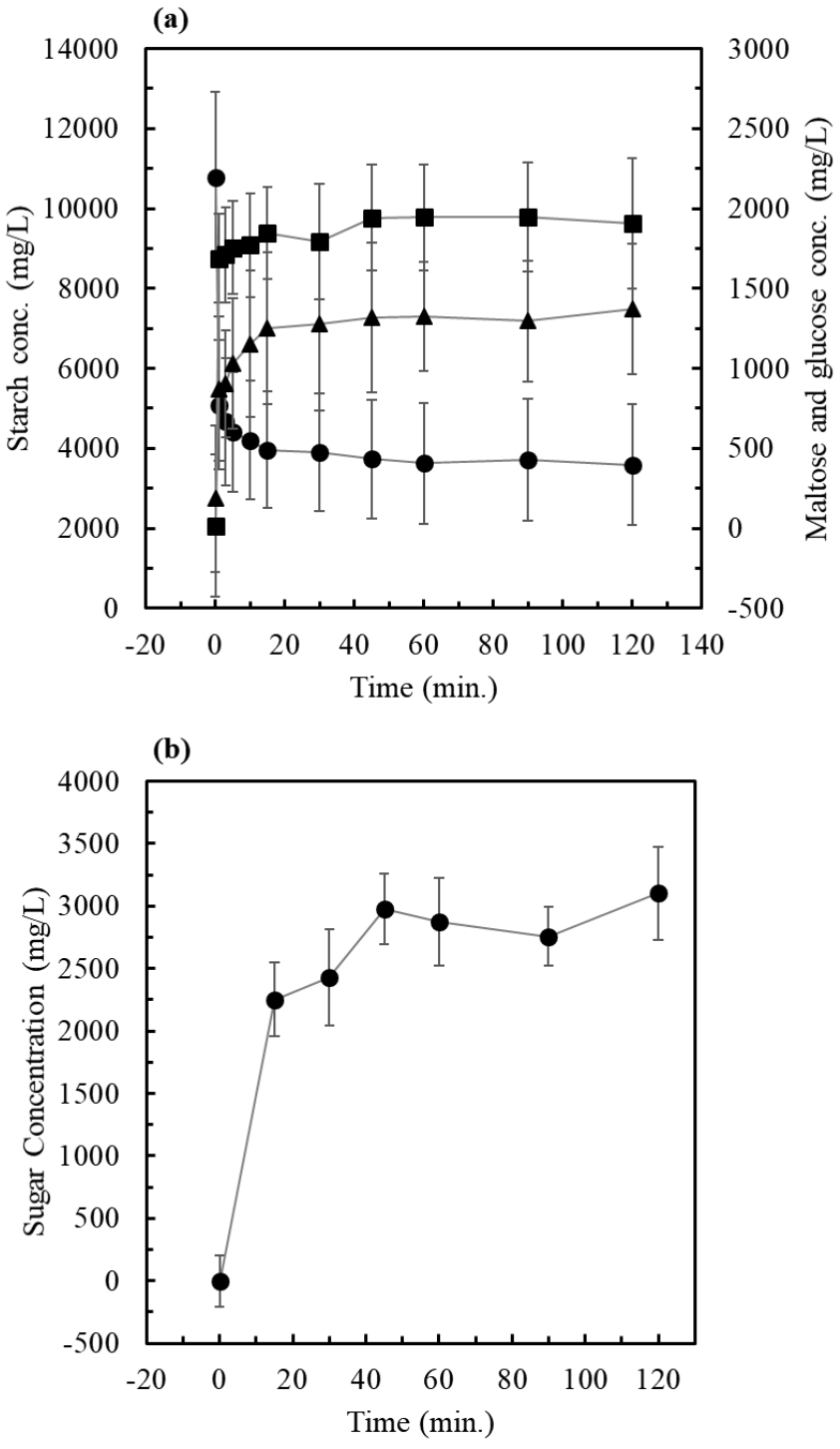

Fig. 2 Concentration estimation of starch (●), maltose (■), and glucose (▲) in the reaction with enzyme, α-amylase, by PLSR analysis (a). Concentration estimation of reduction sugar by Miller method (DNSA reagent and UV spectroscopy) (b).

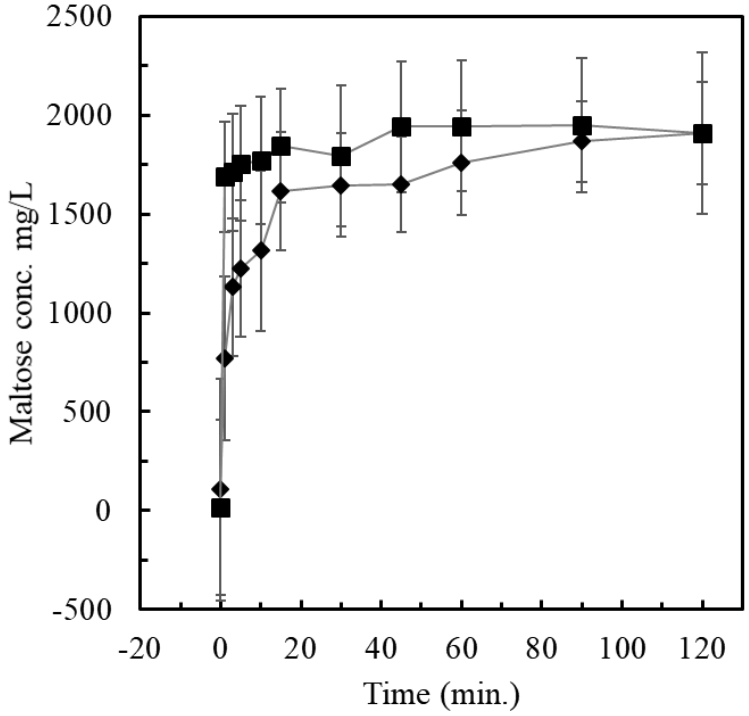

Fig. 3 Concentration estimation of maltose in the reactions at 25℃ (■) and 10℃ (♦).

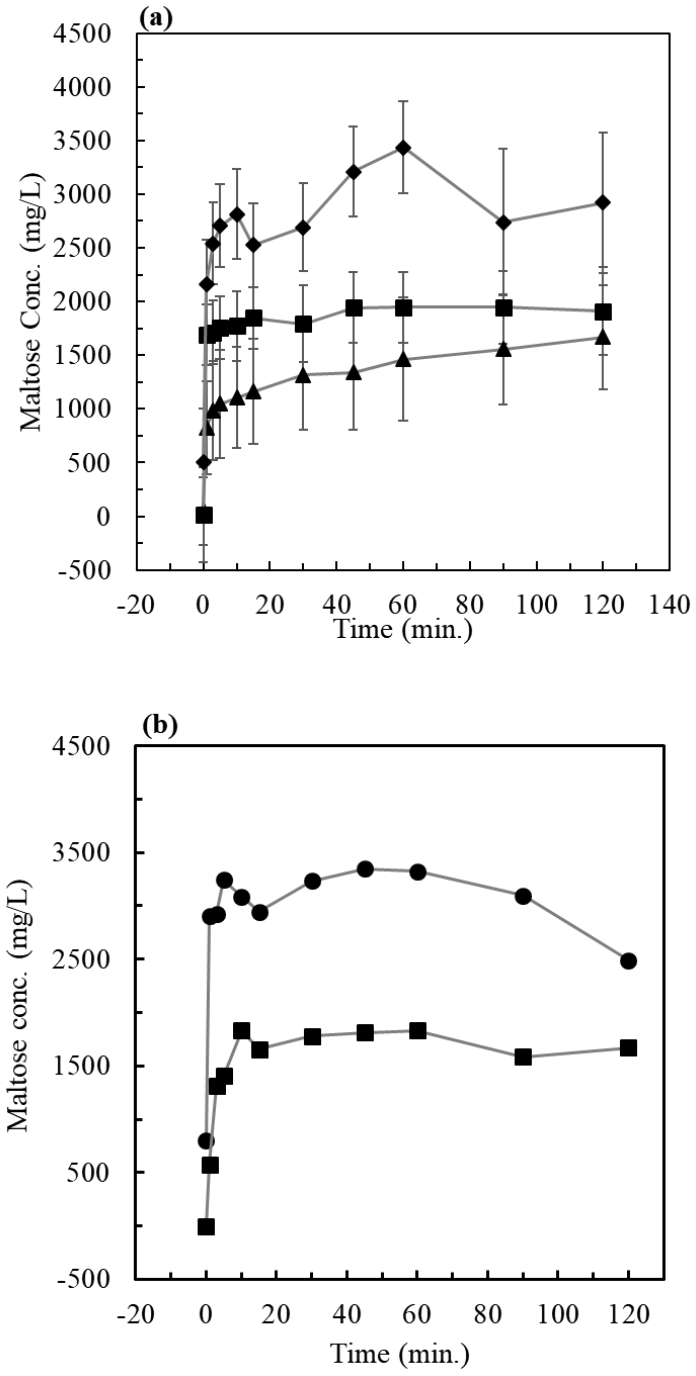

Fig. 4 Concentration estimations for maltose (■) and glucose (▲) in the α-amylase reaction with adding 1,000 mg/L (♦) maltose at the initial reaction measured by PLSR analysis (a) and that by Miller method (b). The line (■) shows maltose concentration analyzed without adding excess maltose (Same to the line of maltose in Fig. 3).

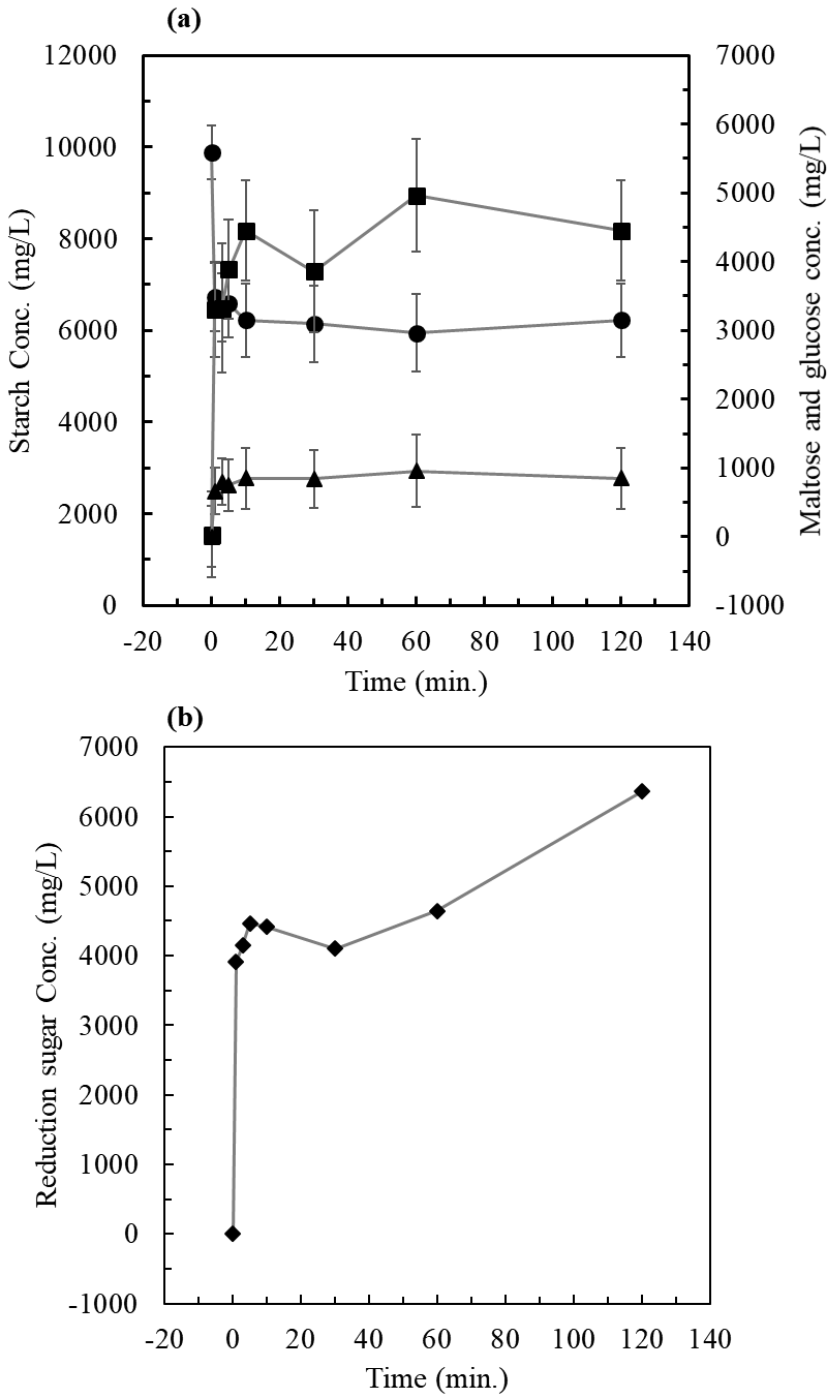

Fig. 5 Estimation of the concentration of starch (●), maltose (■), and glucose (▲) in the reaction with β-amylase by PLSR analysis (a) and that by Miller's method (b).

	Starch (mg/L)	Maltose (mg/L)	D-glucose(mg/L)
a.	10000	0	0
b.	8000	500	100
c.	6000	1000	500
d.	4000	2000	1000
e.	2000	4000	2000
f.	1000	6000	3000
g.	0	8000	4000

Table 1. List of starch, maltose, and D-glucose concentrations for the test model.

Supplementary information: Detailed description of PLSR models

Figure 1A shows a calibration curve for maltose built using two factors. The loading plots for factors 1 (1) and 2 (2) are depicted in Fig. 2A. A broad feature with two tops at 529 and 580 cm^{-1} appears in the plot of factor 1. Although the band shape of factor 1 is not similar to that of pure maltose, the contribution of factor 1 to the prediction model was high at 57%. PLS model for maltose has high regression square (R^2) up to 0.9644 and 0.926 for test and validation. The calibration model (Fig. 1B) for glucose was built with factors 1–3. The optimized spectral region was from 500–650 cm^{-1}, in which the strong band at 519 cm^{-1} was excluded. The R^2 values are 0.927 and 0.923 for the test and validation data sets. The loading plot of factor 1 (Fig. 2B) shows a gentle slope down to higher frequency and a small shoulder is seen near 541 cm^{-1}, which may be attributed to glucose. The contribution of factor 1 to the calibration model was 98%. This fact indicates that factor 1 reflects the alteration in the band of water having an interaction with glucose. A calibration model and loading plots of factors for starch are shown in Figs. 1C and 2C, respectively. The model was built with only factor 1 and its spectral range was from 465 to 490 cm^{-1}. The spectral range is extremely narrow because it includes only a band at 479 cm^{-1} that is characteristic to starch and, in this range, it does not become overwhelmed with water band and other components. The R^2 values of this model are 0.900 and 0.890 for the test and validation data sets, respectively. The plot of factor 1 resembles of starch band in Fig. 2C.

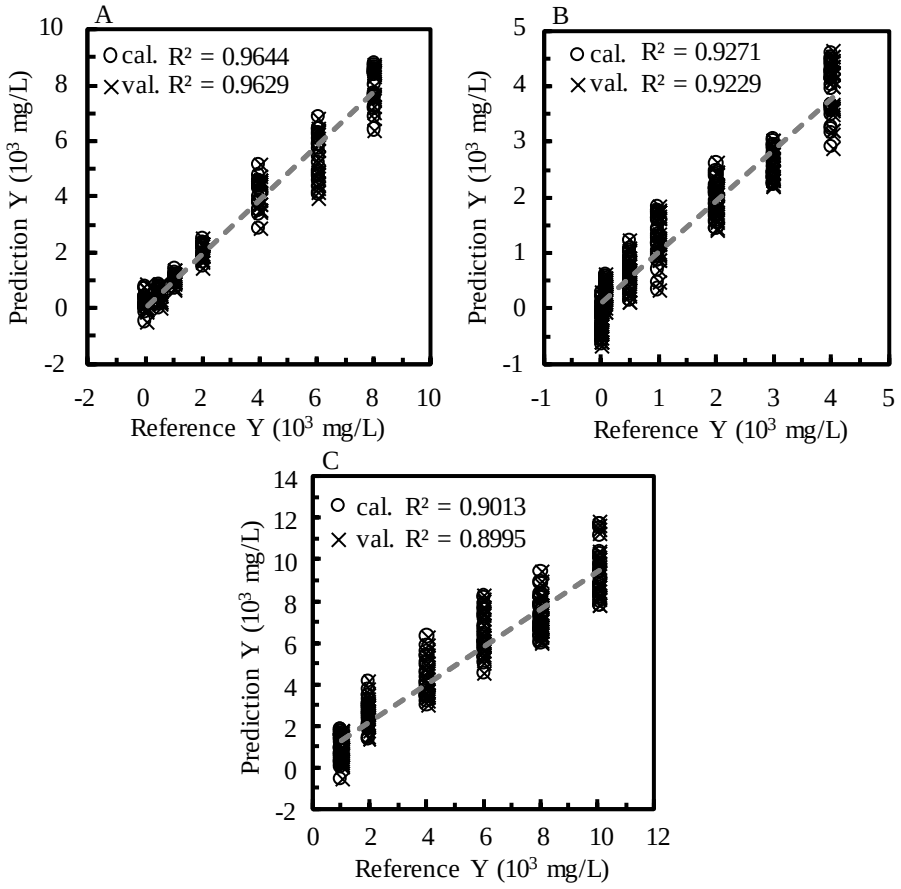

Fig 1. Calibration curves (A, B and C) of the PLSR models to analyze maltose, glucose and starch, respectively.

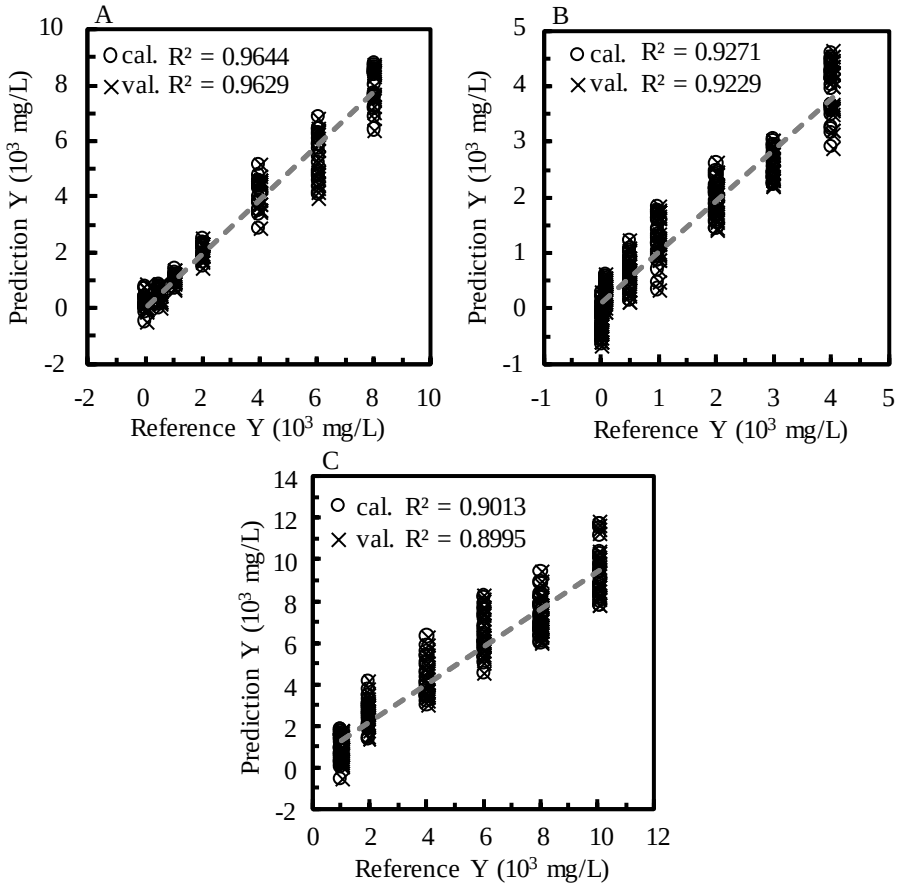

Fig 1. Calibration curves (A, B and C) of the PLSR models to analyze maltose, glucose and starch, respectively.

Chapter 2

Application of Imaging Raman Spectroscopy to study the Distribution of *Kappa* Carrageenan in the Seaweed *Kappaphycus alvarezii*

Abstract

Raman imaging spectroscopy has been applied to analyze carrageenan accumulations in the red algae, *Kappaphycus alvarezii*. The Raman spectra of the sample suggested that the thallus of *K. alvarezii* mainly consists of cellulose and carrageenan. A partial least square regression prediction model for carrageenan semi-quantitative analysis has been built with a simple two-material system and applied to visualize the three dimensional carrageenan distribution in the algal body. The images clearly depicted the differences in carrageenan distribution between carrageenan-rich and -poor samples. Images stained for carrageenan with methylene blue showed results similar to those from analysis with Raman imaging spectroscopy. Our results suggest that Raman imaging spectroscopy is an accurate and useful method for detecting carrageenan distribution in algae.

Keywords

Kappaphycus alvarezii, carrageenan, Raman spectroscopy, chemometrics

Introduction

The seaweed *Kappaphycus alvarezii* is a macro alga belonging to the phylum Rhodophyta, and is abundant in tropical seawater, i.e. on the coasts of Indonesia, Philippines, China, and Vietnam (Ask et al. 2001). The Food and Agriculture Organization (FAO) reported that Indonesia is a major producer of *K. alvarezii*, with a production capacity of up to 10 million tons in 2014. There are many places of seaweed farming in Indonesia, i.e., Karimunjawa, Bali, Sumba, and Sulawesi (Soegiarto and Sulustijo 1990; Manuhara et al. 2016). *K. alvarezii* contains a high weight ratio of carbohydrates (Bixler 1996; Lechat et al. 1997). Carrageenan is sulfated polysaccharide extracted from red algae (Normah and Nazarifah, 2003). The most valuable carbohydrate extracted from *K. alvarezii* is *kappa* (κ)-carrageenan (Fig. 1), which has D-galactose 4-sulfate and 3,6 anhydrous D-galactose residues linked at the β (1,4) and α (1,3) carbons, respectively (Lechat et al. 1997; Rhein-Knudsen, 2015; Cunha and Grenha, 2016). Carrageenan is in high demand in many industries, i.e., food, pharmacy, and cosmetics, owing to its stabilizing, gelling, and thickening properties (Pereira et al. 2013; Necas and Bartosikova, 2013; Azevedo et al. 2013). In the market, there are two types of carrageenan products that are differentiated by quality: semi-refined carrageenan (SRC) and refined carrageenan (RC). SRC and RC use different purification steps such as centrifugation, filtration, and alcohol precipitation (McHugh 2003).

The purpose of the present study is to demonstrate that Raman imaging combined with chemometrics are powerful tools for studying carrageenan distribution in algae. Although the quality and yield of carrageenan production generally depends on the seaweed itself, there is no clear standard for quality control. It is difficult to determine the quality of the seaweed only from its appearance and shape. Currently, extraction is the only method to examine the quality of seaweed farming, but it is destructive and not applicable to study the localization of carrageenan in the algal body. Thus, many researchers in carrageenan industries have keen interest in a tool

that can investigate the quality and quantity of seaweed *K. alvarezii* in raw material.

Vega et al. (2017) reported that fluorescence microscopy can be used to determine the distribution and type of carrageenan in *K. alvarezii*. This method, based on fluorescent labeling, allows the monitoring of micro localization of the target molecule, even in a cell (Henriques et al. 2011; Smith et al. 2016). In contrast, Raman spectroscopy is a label-free technique that can detect chemical changes even within a single cell. Carrageenan and *K. alvarezii* have been extensively studied by Raman and IR spectroscopies (Pereira et al. 2003, 2009, 2013; Pelegrın et al. 2006; Dewi et al. 2012; Webber 2012). Carrageenan is a sulfated polysaccharide, which gives specific bands in both Raman and IR spectra. Pereira (2009) have assigned three strong bands in the range of 1240–1260, 1075–1085, and 845–850 cm^{-1}, due to the vibrational modes of the sulfate ester, galactose, and galactose 4-sulfate, respectively (Table 1).

In the present study, we aimed to analyze the distribution of carrageenan in three different branch sizes of *K. alvarezii* using Raman imaging technique. Raman spectroscopy has been applied for the semi-quantitative analysis of specific materials in intact biological samples (Meksiarun et al. 2015, 2016). Since Raman spectroscopy is a vibrational spectroscopy, all molecules present in the biological matrix display fingerprint bands of their chemical component in the Raman spectrum, unlike in absorption or fluorescence spectroscopy. However, it is necessary to apply multivariate analysis to extract information on a specific molecule in the Raman spectrum. The classical least square (CLS) method or least square curve fitting method is often used for quantitative analysis. Since it is based on a linear combination of spectra of major components included in the sample, the analysis does not require any prediction model and sample preparation, except for measurement of the component spectra. CLS, however, requires full knowledge of all components in the training samples of the measured system (Nadler and Ronald 2005). In contrast, partial least

square regression (PLSR) analysis is another powerful quantitative method, which builds a robust prediction model for targeted material. Unlike the CLS method, it works with only knowledge of the substance of interest. Therefore, PLSR analysis is useful for the analysis of noisy spectra. Raman imaging is useful for studying the distribution of a component in a sample (Ishigaki et al. 2017). In this imaging technique, the Raman spectrum could be obtained from each measurement point, which covers the whole sampling area with spot-to-spot spatial intervals. Consequently, one Raman image consists of many Raman spectra, which composes a hyperspectral image. To reduce the total measuring time, it is necessary to reduce the acquisition time at each sampling spot, resulting in the relatively noisy feature of the spectra. This suggests that the PLSR analysis is suitable in the present study, owing to the noise and perturbation compared to other multivariate analyses, such as CLS.

Material and method

Sample Preparation

Sun dried *K. alvarezii* sampled in two farming areas (Karimunjawa and Sumbawa, Indonesia) was used. Samples were washed with purified water for three times to remove dust, sand, and crystal salt, and soaked in 3.5% NaCl water overnight. Several 2-mm-thick samples were sliced with a knife to obtain Raman images. Three samples were obtained from different places on each plant ((a) first, (b) second, and (c) third branches) of the seaweed as shown in Fig. 2. Refined κ-carrageenan was purchased (Wako pure chemical, Japan) and used without further purification. Powdered methylene blue (MB; Waldeck, Germany) was dissolved in purified water with 3.5% (w/v?) NaCl to prepare the 0.05% (w/v) aqueous solution. The same sliced sample, often the Raman measurement, was soaked in the solution for 30 minutes, and then rinsed with purified water three times. Carrageenan distribution was observed using methylene blue, as previously described (Campo et al. 2009).

Raman Measurement

The InVia Raman System (Renishaw Inc., UK) with a 785 nm excitation laser was employed to obtain 2D and 3D images. A homemade aluminum stage with water reservoirs was used for image measurement to keep the samples from drying. The cross-sectioned sample was fixed on the aluminum stage and soaked in 3.5% NaCl. The spectra of test samples for PLSR analysis were obtained with the streamline mode of the instrument, which employs a line-focused laser light for excitation with a 20 × magnification objective lens. The laser power was 190 mW at the sampling point. For the 2D and 3D imaging measurement, we used the confocal mode of the instrument. Data were collected at sampling points, with intervals of 250 μm for the X- and Y-axes and 50 μm for the Z-axis. The exposure time was 3 s at every sampling point. It took approximately 3–5 h for each sample to obtain 2D or 3D images.

Chemometrics analysis

To analyze the concentration of carrageenan, a PLSR model was built with 11 test samples that were prepared with carrageenan and cellulose powder (Mahardika et al. 2018). Carrageenan and cellulose powders were mixed and ground with a hand homogenizer. The mixed carrageenan – cellulose test sample was placed on a metal substrate and pressed to make a small tablet. One hundred Raman spectra points were obtained at each tablet. All Raman spectra from samples were processed by interpolation, background subtracted, sixth polynomial baseline corrected, normalized by CH band at 1470 cm^{-1}, and smoothed using a Savitzky-Golay second order polynomial with 25 points on both sides of the frequency. The PLSR model was built using Unscrambler 10.1 software (CAMO Software AS., Oslo, Norway).

Results

The Raman spectra of the inner (a) and outer (b) layers of the algae branch were compared to those of cellulose (c) and refined carrageenan (d) in Fig. 3A. A bright-field image of the sample is shown in Fig. 3B, where the sampling point of the inner (a) and outer (b) layers are marked with arrows. The PLSR analysis was employed to quantify the concentration of carrageenan in the algal body. A calibration curve of the PLSR prediction model built with only factor 1 is shown in Fig. 4A. The loading plot of factor 1 shows bands from carrageenan in a positive direction and those from cellulose in a negative direction (Fig. 4B). The regression square (R^2) of the one-leave-out cross validation was 0.9935 and its root mean square error (RMSE) was 0.0275.

A hyperspectral Raman image was obtained to estimate the distribution and concentration of carrageenan in the seaweed branches. The measurement mode was changed to the confocal setup that has a high spatial resolution: 250 μm in the lateral direction and 50 μm depth. The PLSR prediction model was applied to the hyperspectral image to obtain a topological map of carrageenan distribution. Figure 5 depicts the carrageenan distribution (A) in the three branches at -100 μm depth. A bright field image of the cross-sections of branches (B) shows no specific signal for carrageenan, indicating that it is impossible to estimate the concentration of carrageenan from its visual appearance. Fig. 5C shows the carrageenan concentration in the cross-section near 4,000 μm on the Y-axis in the image (shown as a bright red line in Fig. 5A).

Figure 6 shows the carrageenan distribution (A) in a carrageenan-poor branch. A bright field image (B) shows a similar feature to that of the carrageenan-rich branch (Fig. 5B), suggesting that it is very difficult to estimate the concentration of carrageenan with the shape of the branch. The carrageenan concentration in the cross-section was near 3,000 μm on the Y-axis in the image. The carrageenan concentration predicted by PLSR analysis in this cross-section was a maximum of 10% in both the first and second branches. The average carrageenan concentration in the first

branch of the carrageenan-poor branch was only 4.5%.

Three-dimensional (3D) mapping images of the carrageenan concentration for the carrageenan-rich (A) and -poor (B) samples are depicted in Fig. 7. It should be noted that the carrageenan distribution was analyzed at 250 μm below the surface in a nondestructive manner. For the comparison of carrageenan distribution study, MB staining methods were employed. MB staining is a useful method for determining carrageenan and other anionic hydrocolloids (Soedjak 1994; Campo et al. 2009). MB has the characteristics of a cation; it easily binds to anions. The sulfate group in carrageenan has the characteristics of an anion because of its negative charge, which enables binding with MB. The MB staining of *K. alvarezii* of the first (a), second (b), and third (c) branches are shown in Fig. 8.

Discussion

There were either no or very few features observed in the Raman spectroscopy at a frequency region higher than 1600 cm^{-1}, except for a broad band due to OH groups near 1640 cm^{-1} (Fig. 3A). This suggests that the algae contain very little lipids and proteins. Although *K. alvarezii* is a red alga that generally has carotenoid species, such as zeaxanthin and β-carotene, there were no carotenoid bands observed in the Raman spectra (Indriatmoko et al. 2015). Since the sample was dried under the sun, pigments in the sample would be reduced. Additionally, the excitation light at 785 nm has either no or a very weak resonance enhancement effect for carotenoids (Sato et al. 2001). Strong bands at 1122 and 850 cm^{-1} are good marker of cellulose and carrageenan (Fig. 3). Cellulose is a major component of the cell walls of the algae; therefore, the spectrum of the outer layer has a relatively strong contribution of cellulose, which is observed as a shoulder band. In contrast, a strong band at 850 cm^{-1} of carrageenan was observed in both the inner and outer layers of the branch. The spectra of the cross-sectioned branch have strong contributions from

carrageenan, suggesting that *K. alvarezii* produces high concentrations of carrageenan. According to literature the band at 850 cm^{-1} have been assigned to a vibrational mode of galactose 4-sulfate (G4S) (Pereira et al. 2009).

More than 50% of the dry weight of *K. alvarezii* comes from carbohydrates, including cellulose and carrageenan (Lechat et al. 2000; Vreeland and Kloareg 2000; Masarin et al. 2016). A PLSR prediction model was built with a series of 11 mixed κ-carrageenans and cellulose at different ratios (Fig. 4A) (Mahardika et al. 2018). Carrageenan is insoluble in both room temperature (25 ^{0}C) water and most organic solvents; it was not possible to make a homogenous mixture solution of the artificial test samples to build a calibration model, though they are microstructures in the algal body. Therefore, fine powders of materials were used to obtain the concentration-controlled mixed samples. Since the particle size was relatively large (~1 μm) compared to the spatial resolution of the objective lens, a line excitation mode was employed instead of the confocal mode for the measurement of test samples. There were 11 test samples prepared, and 100 spectra obtained from each sample were used to build the PLSR model (Mahardika et al. 2018)

Raman spectroscopy is a kind of light scattering spectroscopy where the spectral intensity is affected by interference and sample conditions, such as scattering and absorption of the sample, and by instrumental instability, such as the distance between the sample and objective lens, laser power, and stray light. Therefore, an independent internal standard is necessary for Raman spectroscopy to obtain the absolute concentration of a sample. Instead, we employed a semi-quantitative analysis in this study that gave the relative concentrations of the targeted material. Intensity correction was performed on all Raman spectra in the hyperspectral image with a standard band at 1470 cm^{-1}, that was assigned to a CH bending mode of which represents all bio-organic

materials, because they generally have CH groups. In the present test sample system, the concentration of carrageenan had a high collinearity with that of cellulose, which is usually avoided when building a robust theoretical prediction curve. However, it is acceptable in the case of semi-quantitative analysis when the system is composed of only two materials (Mahardika et al. 2018). In this case, the increment of the first material is negatively correlated with a decrease in the second material. Therefore, only one factor explains all variables, and the component of the factor that has contributions from the spectrum of the first material is in a positive direction, and from that of the second material is in a negative direction (Fig 4B).

The Raman image in Fig. 5A shows that carrageenan, located in the algal cell wall is mostly distributed in the medullary (inner) portion in all branches corroborating the literature data (Vreeland et al. 1992). In contrast, the carrageenan distribution in Fig. 5A seems to have correlation with the size of the branch (Fig. 5B). The carrageenan concentration in the medullary portion has been found to be the highest in the largest branch and has gradually been reduces towards the peripheral area. These results indicate that the PLSR model can predict carrageenan concentration and distinguish between sample and interval space. The highest carrageenan concentration shown in this cross-section was up to 40%, while the average carrageenan concentration in the first branch (enclosed by the white dashed line) in Fig. 5A was 16%. According to the carrageenan distribution images (Fig. 5 and 6), the average carrageenan concentration was 5–20% in the samples. Masarin et al. (2016) reported that extraction of carrageenan as a sulfated galactan from *K. alvarezii* was in the range of 30–40%. The present sample seems to have relatively lower concentrations compared to these samples.

The advantage of Raman 3D imaging has been demonstrated in the study of carrageenan distribution in the Z-direction. The images in Fig. 7 illustrate that the carrageenan distribution is

significantly altered as the depth increases along the branch. The carrageenan concentration increases at 150 μm in the Z-direction, even in the carrageenan–poor branch (Fig 7B). The 3D images suggest that carrageenan distribution is concentrated in the medullary space, as suggested in the 2D image, but the distribution throughout the depth of the branch shows diversity. This suggests that there are complicated structures for production and accumulation of carrageenan in the longitudinal direction of the branches, and transportation of carrageenan is not active in the algae stem. It may be due to lack of phloem in the organ.

The images of MB staining (Fig. 8) show similar distributions of carrageenan to those estimated by Raman observation. The first branch shows a deep blue color near the medulla portion and less at the cortex portion. Carrageenan seems to be distributed evenly across the second and third branch. The blue color at the outer cortex is the indication of sulfate anion from iota carrageenan (Vreeland et al. 2000). Unfortunately, it is difficult to analyze the concentration and 3D distribution of carrageenan with the MB staining method.

Conclusion

Raman imaging spectroscopy is a nondestructive and label-free analytical tool that can be applied to investigate carrageenan production in *K. alvarezii*. No fluorescence and strong resonance Raman bands interference was observed due to pigments in the sun dried seaweed when the Raman measurement has been performed. The PLSR prediction model, made of simple test samples of only carrageenan and cellulose, successfully illustrates carrageenan concentrations in the 3D images of seaweed. The present results demonstrate that Raman imaging spectroscopy has the potential to investigate saccharide present in the algal body and to evaluation the quality of carrageenan-producing seaweed plantations.

References

Ask EI, Batibasaga A, Zertuche-González JA, San M de (2003) Three decades *of Kappaphycus alvarezii* (Rhodophyta) introduction to non-endemic locations. Proceedings of the 17th International Seaweed Symposium, South Africa, pp 49-57.

Azevedo G, Hilliou L, Bernardo G, Pinto IS, Adams RW, Nilsson M, Villanueva RD (2013) Tailoring kappa/iota-hybrid carrageenan from *Mastocarpus stellatus* with desired gel quality through pre-extraction alkali treatment. J of Food Hydrocol 31:94–102.

Campo VL, Kawano DF, da Silva Jr DB, Carvalho I (2009) Carrageenans: Biological properties, chemical modifications and structural analysis– A review. Carbohydr Polym 77:167–180.

Cunha L, Grenha A (2016) Sulfated seaweed polysaccharides as multifunctional materials in drug delivery applications. Mar Drugs 14:42.

Dewi EN, Darmanto YS, Ambariyanto (2012) Characterization and quality of semi refined carrageenan (src) products from different coastal waters based on fourier transform infrared technique. J Cos Dev 16(1):25-31.

Freile-Pelegrín Y, Robledo D, Azamar JA (2006) Carrageenan of *Eucheuma isiforme* (Solieriaceae, Rhodophyta) from Yucata´ n, Mexico. I. effect of extraction conditions. Bot Mar 49:65–71

Henriques R, Griffiths C, Rego EH, Mhlanga MM (2011) PALM and STORM: Unlocking live-cell super-resolution. Biopolymers 95 (5):322-331.

Indriatmoko, Heriyanto, Limantaraa L, Brotosudarmo HTP (2015) Composition of photosynthetic pigments in a red alga *Kappaphycus alvarezi* cultivated in different depths. Procedia Chemistry 14:193 – 201.

Ishigaki M, Meksiarun P, Kitahama Y, Zhang L, Hashimoto H, Genkawa T, Ozaki Y(2017) Unveiling the aggregation of lycopene in vitro and in vivo: UV−vis, resonance Raman, and raman imaging studies. J Phys Chem B 121:8046-57.

Lechat H, Amat H, Mazoyer J, Gallant DJ, Buléon A, Lahaye M (1997) Cell wall composition of the carrageenophyte *Kappaphycus alvarezii* (Gigartinales, Rhodophyta) partitioned by wet sieving. J Appl Phycol 9:565–572.

Mahardika A, Andriana BB, Susanto AB, Matsuyoshi H, Sato H (2018) Development of Quantitative Analysis Techniques for Saccharification Reactions Using Raman Spectroscopy. Appl Spectrosc 0(0): 1-7.

Manuhara GJ, Praseptiangga D, Riyanto RA (2016) Extraction and characterization of refined *K-carrageenan* of red algae [*Kappaphycus alvarezii* (Doty ex P.C. Silva, 1996)] originated from Karimun Jawa Islands. Aquatic Procedia 7:106 – 111.

McHugh DJ (2003) A guide to the seaweed industry. Food and Agriculture Organization of the United Nations, Rome.

Meksiarun P, Spegazzini N, Matsui H, Nakajima K, Matsuda Y, Sato H (2015) In vivo study of lipid accumulation in the microalgae marine diatom *Thalassiosira pseudonana* using Raman spectroscopy. Appl Spectrosc 69:45-51.

Meksiarun P, Andriana BB, Matsuyoshi H, and Sato H (2016) Non-invasive quantitative analysis of specific fat accumulation in subcutaneous adipose tissues using Raman spectroscopy. Sci Rep 6:37068.

Nadler B, Coifman RR (2005) The prediction error in CLS and PLS: the importance of feature selection prior to multivariate calibration. J Chemom 19:107–118.

Necas J, Bartosikova L (2013) Carrageenan: A review. Vet Med 58(4):187–205.

Normah O, Nazarifah I (2003) Production of semi-refined carrageenan from locally available red seaweed, *Eucheuma cottonii* on a laboratory scale. J Trop Agric and Fd Sc 31(2):207–213.

Pereira L, Sousa A, Coelho H, Amado AM, Ribeiro-Claro PJA (2003) Use of FTIR, FT-Raman and 13C-NMR spectroscopy for identification of some seaweed phycocolloids. Biomol Eng 20:223-228.

Pereira L, Amado AM, Critchley AT, van de Velde F, Ribeiro-Claro PJA (2009) Identification of selected seaweed polysaccharides (phycocolloids) by vibrational spectroscopy (FTIR-ATR and FT-Raman). Food Hydrocoll 30:1-7.

Pereira L, Gheda SF, Ribeiro-Claro PJA (2013) Analysis by vibrational spectroscopy of seaweed polysaccharides with potential use in food, pharmaceutical, and cosmetic industries. Int J Carbohydr Chem. 2013: 7p.

Rhein-Knudsen N, Ale MT, Meyer AS (2015) Seaweed hydrocolloid production: An update on enzyme assisted extraction and modification technologies. *Mar Drugs* 13: 3340-59.

Sato H, Chiba H, Tashiro H, Ozaki Y (2001) Excitation wavelength-dependent changes in Raman spectra of whole blood and hemoglobin: comparison of the spectra with 514.5-, 720-, and 1064-nm excitation. J Biomed Opt 6: 366-370.

Smith R, Wrightb KL, Ashton L (2016) Raman spectroscopy: an evolving technique for live cell studies. Analyst 141: 3590–3600.

Soedjak SH (1994) Colorimetric determination of carrageenans and other anionic hydrocolloids with methylene blue. Anal Chem 66 (24): 4514–18.

Soegiarto A, Sulustijo (1990) Utilization and farming of seaweeds in Indonesia. In Dogma IJ Jr, Trono GC Jr, Tabbada RA (Ed) Culture and use of algae in southeast asia, Proceedings of the Symposium on Culture and Utilization of Algae in Southeast Asia, 8-11 December 1981, Philippines, pp 9-19.

Vega GB, Ceballos JA, Anzalone A, Digman MA, Gratton E (2017) A laser-scanning confocal microscopy study of carrageenan in red algae from seaweed farms near the Caribbean entrance of the Panama Canal. J Appl Phycol 29:495–508.

Vreeland V, Zablackis E, Laetsch WM (1992) Monoclonal antibodies as molecular markers for the intracellular and cell wall distribution of carrageenan epitotes in *Kappaphycus alvarezii* (Rhodophyta) during tissue development. Journal of Phycology, 28:328342

Vreeland V, Kloareg B (2000) Cell wall biology in red algae: Divide and conquer. Journal of Phycology, 36(5):793–797.

Webber V, De Carvalho SM, Ogliari PJ, Hayashi L, Barreto PLM (2012) Optimization of the extraction of carrageenan from *Kappaphycus alvarezii* using response surface methodology. Ciênc. Tecnol. Aliment Campinas 32(4):812-818.

Figures

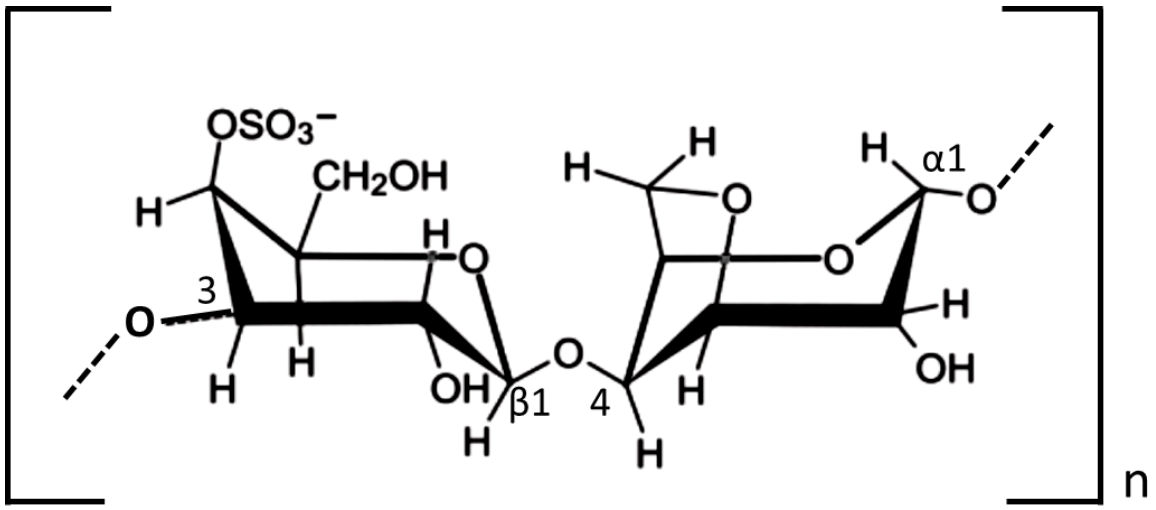

Fig 1. Chemical structure of monomer unit in kappa (κ)-carrageenan

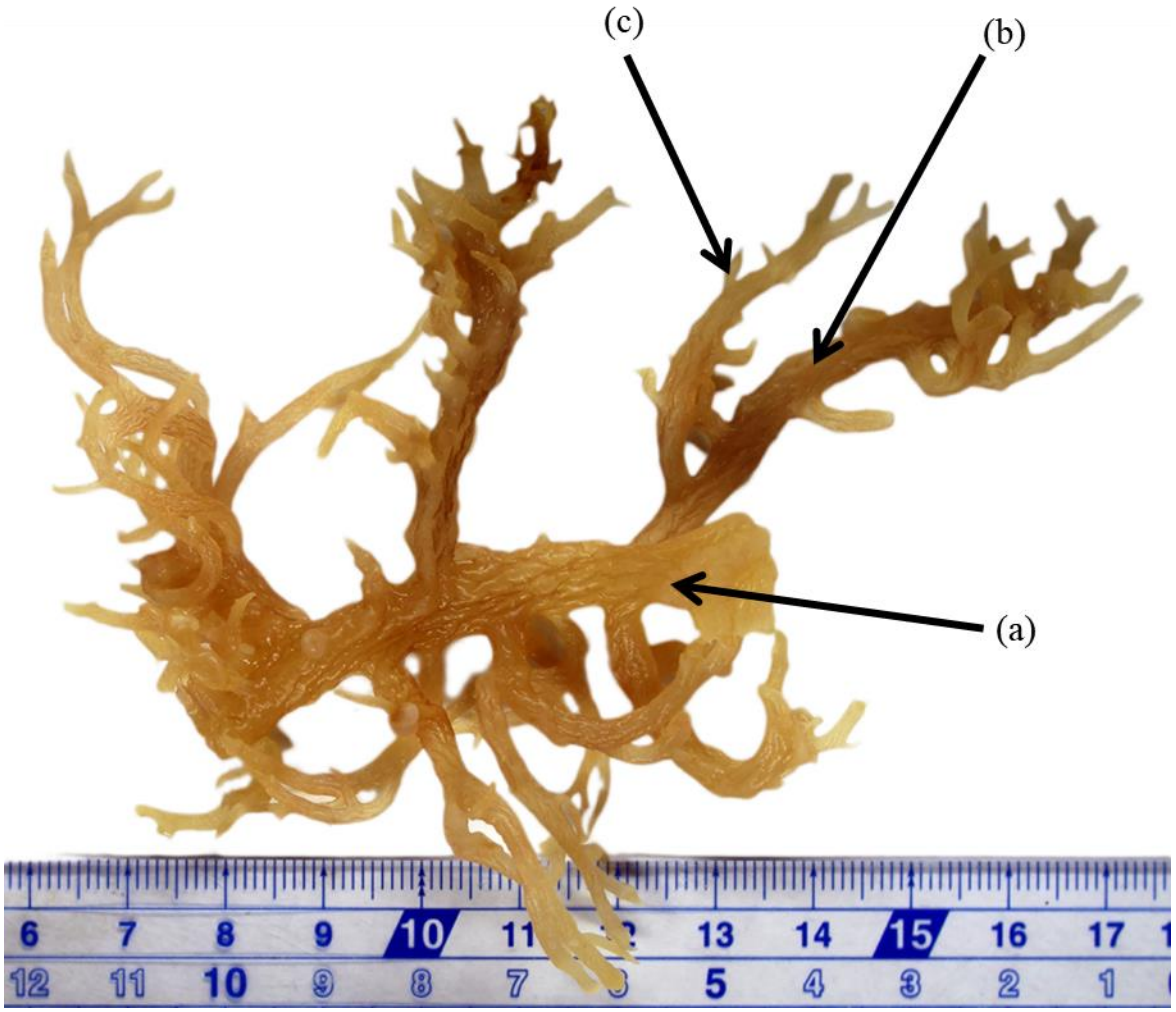

Fig 2. A photo of the sample, *K. alvarezii*. The arrows indicate the first (a), second (b), and third (c) branches.

A

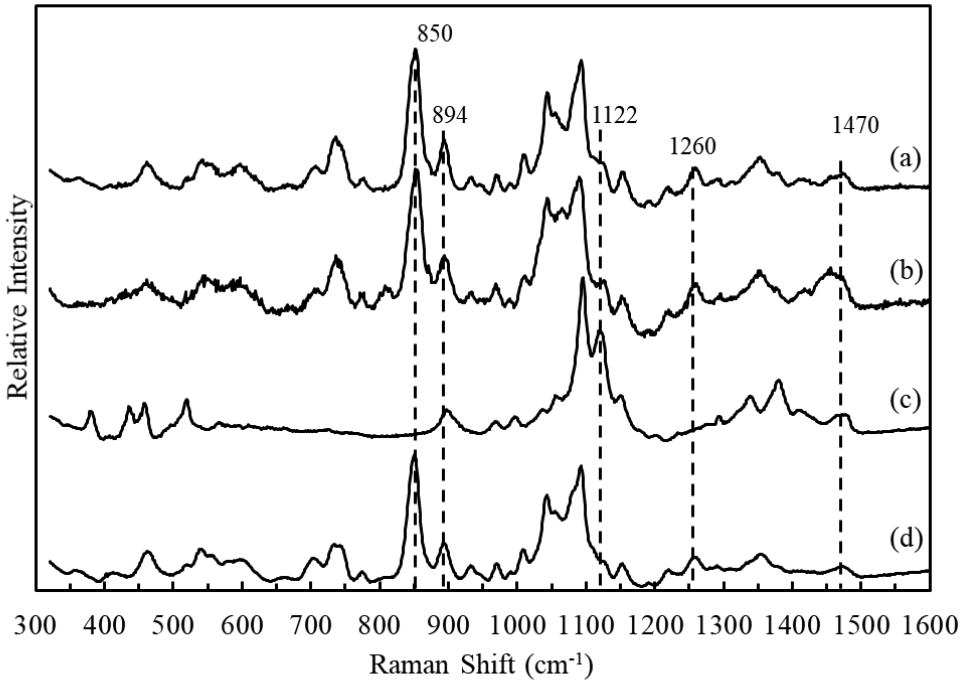

B

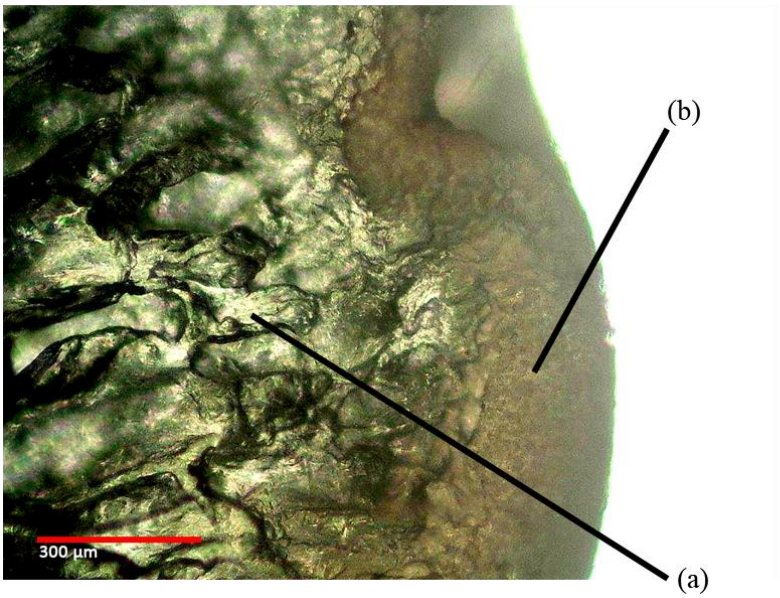

Fig 3. Raman spectra (A) and bright-field image (B) of the cross-section of the first branch. The spectra are the medullary portion (a), outer surrounding portion (b), pure cellulose (c), and refined carrageenan (d). The arrows in (B) indicate selected points for Raman measurements of the medullary (a) and outer surrounding portion (b).

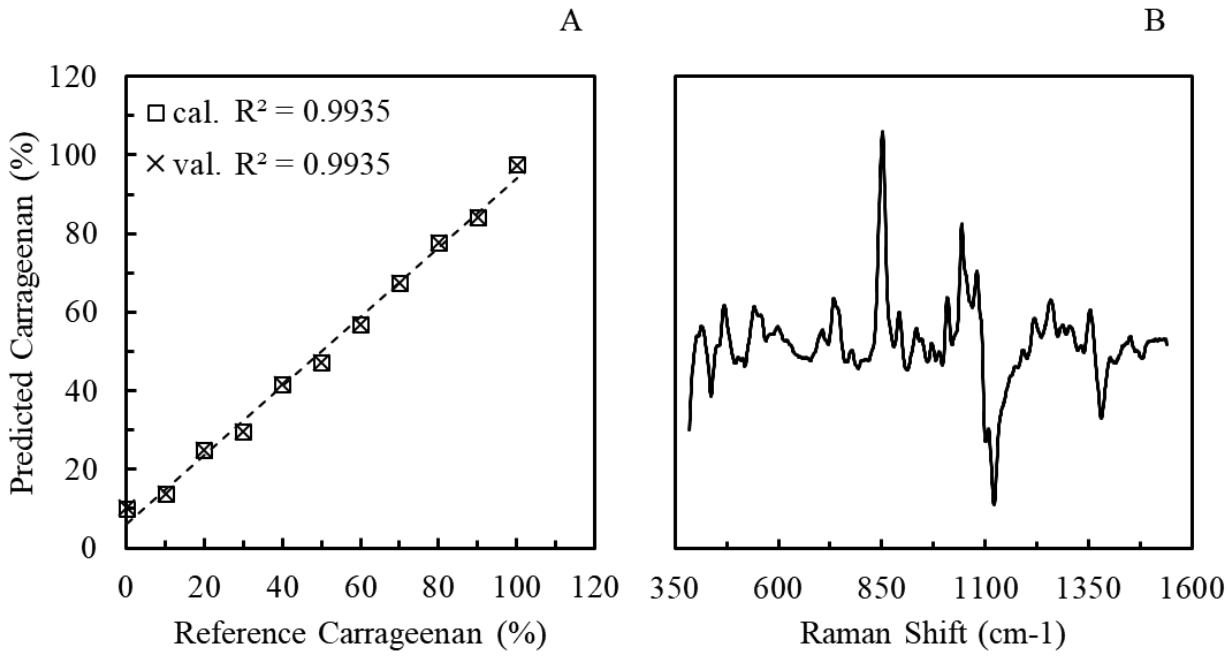

Fig 4. Calibration curve (A) of the PLSR prediction model for cellulose-carrageenan mixed test samples and the loading plot of factor 1 (B).

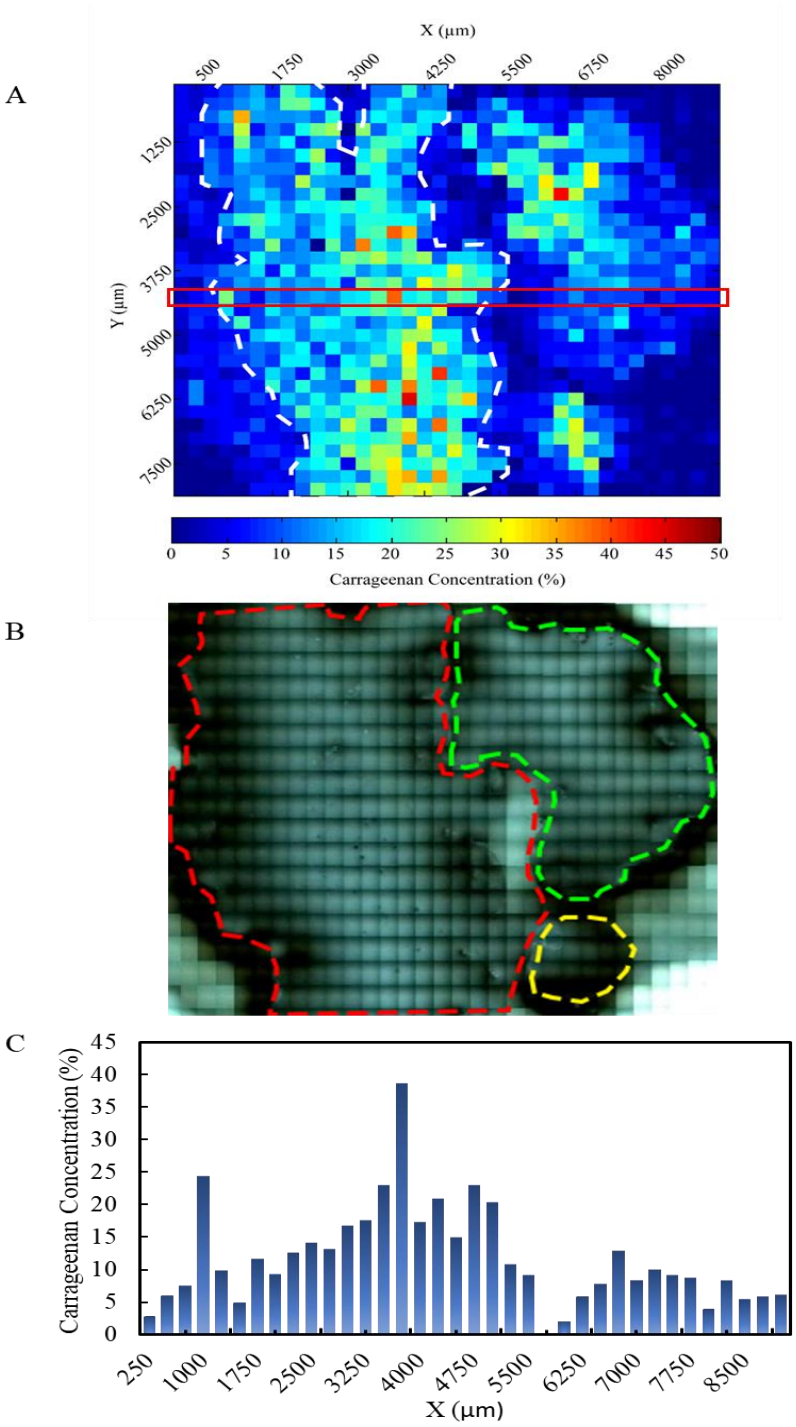

Fig 5. Topographic image of carrageenan distribution (A) and bright-field image of the carrageenan-rich branches (B). The first, second, and third branches are shown with red, green, and yellow dotted lines, respectively. A graph (C) shows the carrageenan concentration along with the horizontal line at 3000 μm on the Y-axis.

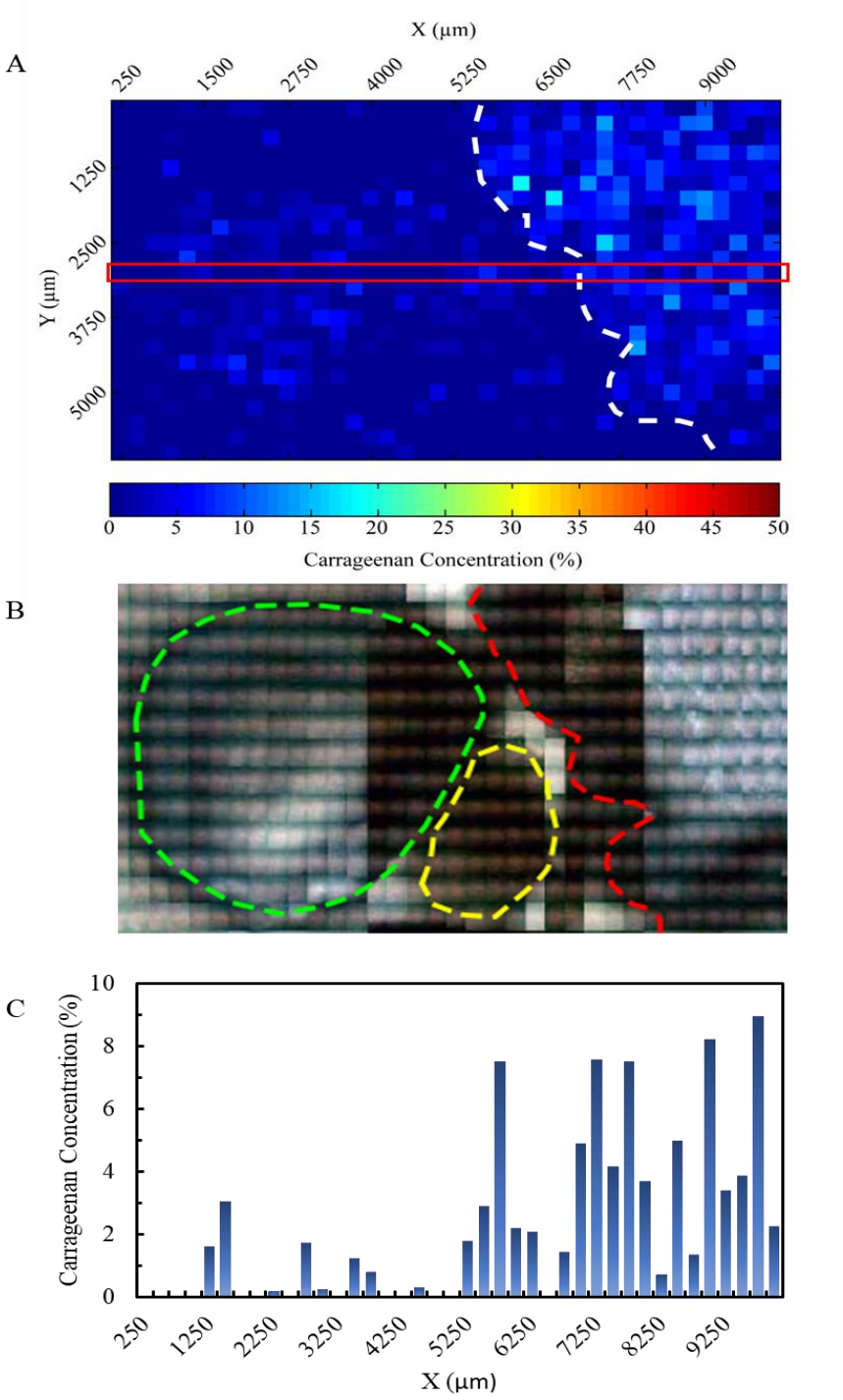

Fig 6. Topographic map of carrageenan distribution (A) and bright-field image of the carrageenan-poor branches (C). The first, second, and third branches are shown with red, green, and yellow dotted lines, respectively. A graph (C) represents the carrageenan concentration for the horizontal line at 3750 μm on the lateral Y-axis.

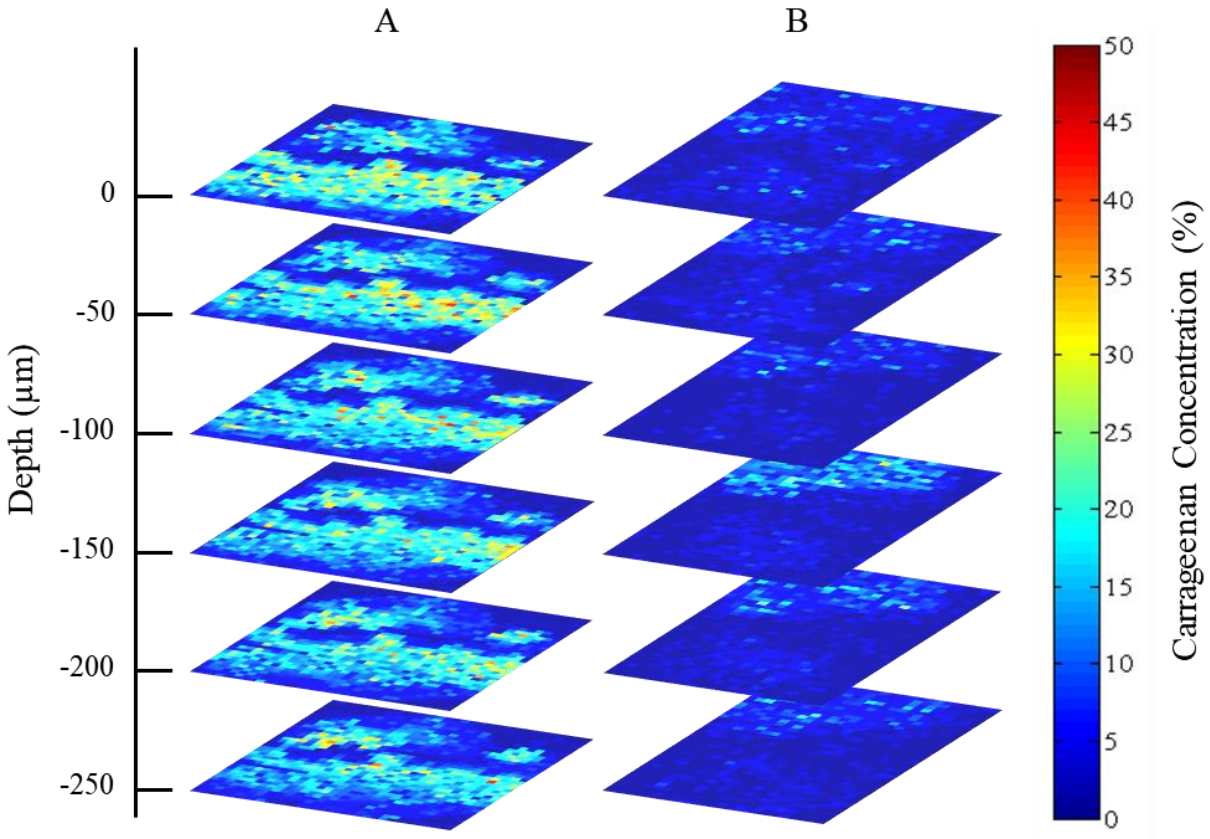

Fig 7. 3D Raman images of carrageenan-rich (A) and -poor (B) branches.

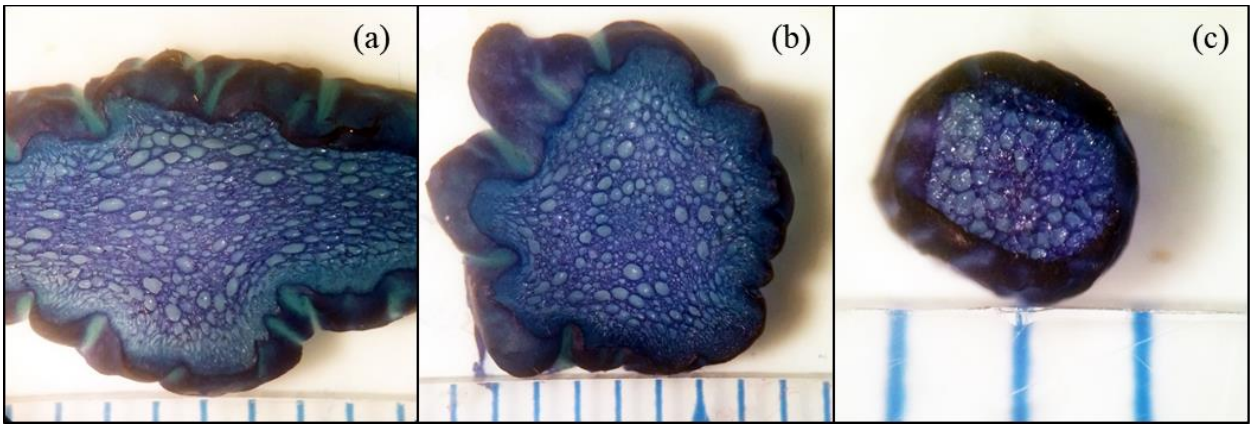

Fig 8. Methylene blue-stained images of carrageenan on the first (a), second (b) and third (c) branches.

Wavenumbers (cm^{-1})	Bond(s)/group(s)	Letter code	Kappa
1240–1260	S=O (sulfate ester)		++
1075–1085	C–O (3,6-anydrogalactose)	DA	+++
970–975	Galactose	G/D	+
925–935	C–O (3,6-anydrogalactose)	DA	-
905–907	C–O–SO_4 (C2-3,6-anydrogalactose)	DA2S	-
890–900	Unsulfated β-D-galactose	G/D	-
867–871	C–O–SO_4 (C6-galactose)	G/D6S	-
845–850	C–O–SO_4 (C4-galactose)	G4S	++
825–830	C–O–SO_4 (C2-galactose)	G/D2S	-
815–825	C–O–SO_4 (C6-galactose)	G/D6S	-
804–808	C–O–SO_4 (C2-3,6-anydrogalactose)	DA2S	-

adapted and modified from Pereira, 2009

Table 1. Characterization of κ-type carrageenan by Raman spectroscopy.

Chapter 3

Bacterial decomposition of Seaweed *Kappaphycus Alvarezii* studied by 3D Raman Imaging Spectroscopy

Abstract

Seaweed diseases are detrimental to the carrageenan industry. One of the major carrageenan sources is *Kappaphycus alvarezii,* which contributes about 97.83% of the total product in the world. *Ice-ice* disease is caused by bacterial pathogens infecting algae weakened by environmental stresses, such as temperature, salinity, sunlight, and nutrients of the sea water. The decreasing carrageenan production is caused by the extracellular enzymatic reaction of the bacteria. To study enzymatic reaction on the algal body, Raman imaging spectroscopy combined with PLSR analysis was employed as a quantitative tool. Candidate bacteria expressing enzymes able to decompose seaweed were collected from putrid algae. Then, the bacteria were isolated and purified and finally applied to the algal body and investigated using Raman image analysis. The reduction in carrageenan concentration was observed in the algae treated with one of the bacteria. The results suggest that the bacteria infect into the algal body and then enzymatically degrades the carrageenan. Observation made by methylene blue staining were in agreement with this hypothesis.

Keywords

Enzyme, carrageenan, Raman spectroscopy, PLSR analysis

Introduction

Seaweed *Kappaphycus alvarezii*, of the Rhodophyta, is one of the most important commodities in Indonesia due to the high industrial demand for its product, *kappa* type carrageenan (Lechat et al. 1997; Rhein-Knudsen 2015; Cunha and Grenha 2016). Carrageenan is a valuable carbohydrate owing to its stabilizing, gelling, and thickening properties (Pereira et al. 2013; Necas and Bartosikova, 2013; Azevedo et al. 2013). It is widely used in industries such as cosmetic, food, pharmaceutical, and so on. *K. alvarezii* is widely spread in the oceans of tropical areas and is especially abundant in Southeast Asia, i.e., the Philippines, Vietnam, Thailand, China, and Indonesia (Ask et al. 2001). The minister of maritime and fisheries of Indonesia reported that seaweed *K. alvarezii* contributes about 97.83% of the seaweed production in the world. In the carrageenan industry, quality control of seaweed farming becomes more important day by day.

Disease of algae is one of the largest problems in carrageenan production. The most famous seaweed disease in tropical seawater is the *ice-ice* disease (Largo et al.1995). It is an inclusive term of a disease caused by a several bacteria, which results in thallus bleaching and even falling off (Mendoza et al. 2002). The *ice-ice* disease was first discovered in a commercial seaweed plantation in Philippine in 1974 (Largo et al. 1995.). Mendoza et al. (2002) also reported that *ice-ice* disease causes remarkable reduction, up to 40%, of carrageenan production. Decreasing seaweed production is due to the loss of seaweed thallus as the cell walls are degraded by enzymes produced by bacterial pathogens (Distel et al. 2002; Weiner et al. 2008). Bacteria belonging to the genera *Vibrio, Alteromonas, Cytophaga, Flavobacterium*, and *Pseudoalteromonas* produce enzymes capable of depolymerizing polysaccharides (Goecke et al. 2010). Rhein-Knudsen (2015) reported that *k*-carrageenan is hydrolyzed by several enzymes, such as *k*-carrageenanse, sufatase, carratetraose-4-*O* monosulfate-β-hydrolase, and sulfurylase I and II. *Pseudoalteromonas carrageenovora* is the most studied microorganism that is able to produce *k*-carrageenase. The *k*-

carrageenase enzyme belongs to the 16th family of glycoside hydrolases (GH). Potin et al. (1995) purified and analyzed a *k*-carrageenase (EC 3.2.1.83) collected from *P. carragenovora* with the ability to cleave the β-1,4 linkages in carrageenan and produces di- and tetra-saccharides. The size of the oligo-galactans produced by hydrolysis reaction depends on the type of carrageenase (Rhein-Knudsen 2015). The cleavage at α-1,3 or β-1,4 linkage in carrageenan results in the production of two different types of saccharides having opposite orientations (Barbeyron et al., 2000; Lemoine et al. 2009). However, different kind of enzymes are also used in carrageenan industries. For example, Blanco-Pascual et al. (2014) used alcalase to extract carrageenan from *Mastocarpus stellatus*, which has better in gelling properties. An enzyme, cellulose, collected from *Aspergillus niger* was used to destroy the cell walls of the seaweed to release carrageenan in *Eucheuma cottonii* (Varadarajan et al. 2009).

Environmental conditions play an important role in the infection of cultivated seaweed by bacterial pathogens (Case et al. 2011). It is suggested that inadequate environmental conditions at the plantation site, i.e., temperature, salinity, pH, nutrients, and sunshine leads to a weakening of the seaweed facilitating the infection by *ice-ice* bacteria. Furthermore, drastic changes in environmental conditions that exceed the limit of adaptation and tolerance of the seaweed can potentially cause susceptibility to microbial pathogens (Karsten et al. 2001; Toohey and Kendrick, 2007). As previous methods for assessment of bacterial pathogens of seaweed disease (Largo et al. 1995a; 1995b; 1999; Mendoza et al. 2002) always employed destructive techniques, little information has been provided about the mechanisms of bacterial infection and decomposition of the carrageenan products in the algal body.

In the present study, 3D Raman imaging technique with PLSR analysis was applied to monitor the bacterial enzymatic activity in the algal body and dynamics of the bacterial invasion.

Raman spectroscopy is a promising, label-free, non-destructive, and environmentally friendly analytical tool to study living cells and tissues (Teixeira dos Santos et al. 2016). Raman spectroscopy has been extensively applied in the study of seaweed and carrageenan (Malfait et al. 1987; Pereira et al. 2009; 2011; 2013; Rodrigues et al 201), as carrageenan has several characteristic bands in the fingerprint region. Pereira et al. (2009) has assigned three strong bands, at 1240–1260, 1075–1085, and 845–850 cm^{-1}, to the vibrational modes of the sulfate ester, galactose, and galactose 4-sulfate, respectively (Table 1). In my previous study (chapter 2), Raman spectroscopy was successfully applied to observe the 3D distribution of carrageenan in seaweed *K. alvarezii* (Mahardika, 2018). This chapter aims to evaluate the developed technique for seaweed disease monitoring with regard to the faster, label-free, and environmentally friendly characteristics.

Material and method

Bacterial screening

Sun-dried seaweed *Kappaphycus alvarezii* was soaked in water containing 3.5% NaCl and subsequently left under open air for a several days, allowing for infection by natural microorganisms. A small amount of the decomposed sample at the surface of seaweed was collected and dispersed into water containing 3.5% NaCl. The samples with bacteria were spread on a culture dish of marine broth agar (MBA) medium and incubated at 25 ℃ for 24 h. Two independent colonies were collected and inoculated into new dishes with MBA medium. In the present study, the two bacteria were referred to as “red” and “orange” due to their natural colors.

Enzymatic assays

The two bacteria samples were cultured in 10% w/v liquid marine broth medium containing 0.25% w/v carrageenan as the sole source carbon at 25℃. A small portion was collected every 24 h to measure the growth rate. Bacterial density was estimated by measuring the optical density at 600 nm. The samples were centrifuged at 10,000 rpm for 10 minutes to collect crude enzyme in the supernatant. The solution was diluted 2 x with Tris buffer pH 7.2 to a final concentration of 50 mM. Carrageenan was added to a final concentration of 0.25% to act as a substrate for the enzymatic reaction. Enzymatic reactions were conducted at 30℃ for 1 h and subsequently stopped by adding dinitrosalicylic acid (DNSA) and boiling at 100℃ for 10 minutes according to Miller's procedure. The concentration of reducing sugars was estimated according to the absorption at 540 nm.

Infection of *K. alvarezii by* selected bacterial strains

The large thallus of seaweed *K. alvarezii* was sliced to a thickness of 5 mm with a scalpel in order to observe the cross section. The sample was soaked in a liquid containing the cultured bacteria. The sample was rinsed with 3.5% NaCl water three times and exposed to UV light for 30 minutes to eliminate bacterial activity. Then, the thallus sample was observed with a Raman imaging instrument. The Raman image measurements were carried out twice at the 3rd and 5th day. After Raman observation, the sample was treated with a 0.05% w/v methylene blue (Waldeck, Germany) aqueous solution with 3.5% NaCl for 30 minutes and rinsed with purified water three times. The methylene blue stained sample was observed with a normal optical microscope to observe the distribution of carrageenan (Campo et al. 2009).

Bacterial Identification

16-s Genomic DNA were extracted from selected seaweed-decomposition bacteria. Centrifuged cell were suspended by adding 100 µl suspension buffer (10 mM Tris-HCL (pH 8), 1 mM EDTA, 350 mM Sucrose) and vortexed for 1 min. 100 µl lysis buffer (100mM Tris-HCL (pH 8), 20 mM EDTA, 300 mM NaCl, 2% SDS) were added to break the cell wall and 1 µl proteinase to hydrolyze cell protein content. Sample were then incubate at 55^0C for 30 min. and flipped slowly every 10 min. In order to remove all protein content, same amount of last mixture sample phenol/ chloroform/ isoamyl alcohol (PCI) were added. Top layer of sample-PCI solution were moved into new microcentrifuge tube. DNA were precipitated by adding 0.6 time of total sample of Isopropanol and put on ice for 5 min. Sample were then centrifuged for 5 min at 15000 rpm and discard the supernatant. 100 µl distillated water and 1 µl RNAse A were added to remove RNA contamination. Sample were incubated at 37^0C for 30 min. DNA were precipitated by adding 3M sodium acetate and 99% ethanol then seated on ice for 15 min. sample were centrifuged for 25 min. at 14000 rpm then discard the supernatant. 1 ml of 70% ethanol were added and seated on ice for another 15 min. sample were centrifuge for 10 min. at 14000 rpm and discard the supernatant. 50 µl distillated water were added and measure the DNA concentration by NanoDrop 1000.

DNA were amplified by PCR with KOD plus polymerase and a pair of universal primers. Primers 518 F (CCAGCAGCCGCGGTAATACG) and 800 R (TACCAGGGTATCTAATCC) with targeted sequence length was 282 base pair were added in the PCR reaction mix. The PCR temperature cycle condition was as follow: initial denature 98^0C for 3 min; successive denaturation 98^0C for 10 sec; annealing 40^0C for 30 sec; and extension 68^0C for 1 min. 40 sec. Series of denaturation, annealing and extension were repeated until 30 cycles. The PCR products were analyzed by 1 % agarose gel electrophoresis and the result was observed using UV lamp. PCR product were then purified by Fast Gene PCR extraction kit. The purified sample were sequenced

using 3500 genetic analyzers sequencer. The nearly complete 16S rDNA gene sequences were used to search the genetic profile similarity in the NCBI database.

Raman spectroscopy

A PLSR calibration model was built with 11 test samples composed of carrageenan and cellulose. Since these molecules are not water-soluble, fine powders were mixed to prepare the test samples with different concentrations of carrageenan. The Raman measurements were made with the InVia Raman System (Renishaw Inc., UK), which is equipped with a 785 nm laser for excitation. The spectra of the test samples were obtained using the streamline mode of the system, in which the sample was irradiated by a line-focused laser with a ×20 magnification objective lens (0.40 NA, Leica, Germany). The power of the laser was 190 mW at the sampling point.

The 3D Raman images of the algae samples were obtained with the same instrument; however, the confocal mode was used for the observation in order to achieve high spatial resolution. A homemade aluminum substrate with water reservoirs was used to keep the sample size and wet during the measurement. The sliced thallus was placed on the substrate and soaked in water containing 3.5% NaCl. The final 3D images consisted of 3200 sampling points with intervals of 250 μm for lateral direction (X- and Y-axes) and of 50 μm for the depth direction (Z-axis) were obtained. The exposure time was three seconds at every sample point, which amounted to a run-time of about 3 h.

Chemometrics analysis

A PLSR model was built using 11 test sample mixtures of carrageenan and cellulose in order to analyze the carrageenan concentration in the algal body of biological samples (Mahardika, 2018). Carrageenan and cellulose were preliminary grounded by hand with a homogenizer to obtain a small particle size before the sample preparation. The carrageenan and cellulose were

mixed together to make a series of concentrations from 0 to 100 % w/w of carrageenan. (See table 2) The mixed carrageenan-cellulose was placed in a small hole on an aluminum plate and pressed to a small tablet. Spectra measured at hundred sample points of each tablet were averaged to obtain test data. The Raman spectra were processed with interpolation, background, and sixth polynomial baseline corrections before the spectra were normalized to a band at 1470 cm^{-1}. The hyperspectral image data was smoothed using a Savitzky-Golay second order polynomial with 25 points on both sides of the frequency. The PLSR analysis was carried out by Unscrambler 10.1 software (CAMO Software AS., Oslo, Norway).

Results

Growth rate curves are depicted in Fig. 1a for the two independent bacterial colonies (red (a) and orange (b)) isolated from the decomposed seaweed *K. alvarezii* grown in 10% liquid marine broth medium. The growth curves showed a log phase during the first day and seemed to reach to a stationary phase later on. After reaching the maximum at 1 day, the orange bacterium gradually increased, while the red bacterium reduced in population. This result suggests that the orange bacterium is tolerant to the deprivation of nutrients. The two bacteria exhibited slightly different activities in the enzymatic reaction in Fig. 2b. The curves represent concentrations of reducing sugar, the product of carrageenan hydrolysis by bacterial enzymes. During the first two days, the bacteria quickly consumed the reducing sugar indicated by sharp decrease in the sugar concentration. The concentration of reducing sugar remarkably increased at the third day, possibly due to the bacterial production of enzymes to hydrolyze carrageenan into the small sugars needed as a carbon source for their proliferation. The orange bacteria showed higher concentration of reducing sugars at day 3. This suggests that the orange bacteria possess the carrageenan hydrolysis enzymes with a higher activity or that the orange one has greater ability to produce the enzyme.

This may also be the reason why the orange bacteria have higher survival ability under nutrient-poor conditions (Fig. 1a).

Figure 3 compares Raman spectra of seaweed *K. alvarezii* (a), cellulose (b), and carrageenan (c). The strong band at 850 cm^{-1} in carrageenan (c) and *K. alvarezii* (a) has been assigned to a vibrational mode of galactose 4-sulfate (G4S) (Pereira et al. 2009) and used for carrageenan detection. The band at 1122 cm^{-1} in cellulose spectra (b), which appear as small "shoulder" in *K. alvarezii* (a), was deemed to be a good marker for cellulose. The CH band at 1470 cm^{-1} seems to be a shared band that was therefore used for spectral normalization.

PLSR analysis was applied to the hyperspectral images of the algal body infected with bacteria to visualize the localization of bacterial invasion. As it was suggested in the study of bacterial proliferation and sugar decomposition (Fig. 2), the speed of enzymatic decomposition of carrageenan was highly correlated with the bacterial proliferation. The PLSR calibration model was built with 11 test samples and the latent variable was one. The correlation coefficient (R^2) of the one-leave-out cross validation was 0.994 and the root mean square error (RMSE) was 0.0275 (fig 4a). The loading plot of factor 1 is depicted in fig 4b. The spectral feature of the loading plot seems to consist of carrageenan-bands in positive and cellulose-bands in negative.

3D Raman images were repeatedly obtained from the largest sliced branch of *K. alvarezii* at 3rd and 5th days after the infections. The bacterial activity was stopped by washing with 3.5% NaCl and exposed under UV light for 30 minutes before measurement. Topographies of carrageenan concentration for the branches with no (control; a), orange (b), and red (c) bacteria at 3rd day are shown in fig 5. The maps suggest that the carrageenan concentration is lowest in the map of the sample infected with the orange bacteria. The topographies of the branch samples

measured at 5th day are exhibited in Fig. 6. The maps show a clear reduction of carrageenan content in the branch infected with the orange bacteria.

Red and orange bacteria are successfully identified by partial 16S rDNA sequencing. Fig. 7 show the PCR amplification of targeted 16S rDNA gene with a pair universal primers. Band appear on gel electrophoresis is about 282 base pair in red and orange bacteria although red bacteria show brighter then orange bacteria. The nearly complete targeted 16S rDNA gene is also success sequenced as follow: red bacteria (NNNNNNNNNNNTNTTGGGCGTAAGCGCGCGCAGG TGGTTCCTTAAGTCTGATGTGAAAGCCCACGGCTCAACCGTGGAGGGTCATTGGAAA CTGGGGAACTTGAGTGCAGAAGAGGAAAGTGGAATTCCAAGTGTAGCGGTGAAATG CGTAGATATTTGGAGGAACACCAGTGGCGAAGGCGACTTTCTGGTCTGTAACTGACA CTGAGGCGCGAAAGCGTGGGGAGCAAACAGGATTAGATACCCTGGTAANAN) with total sequenced 255 bp and orange bacteria (NNNNNNNGGANTATTGGGCGTAAGCGCGCG CAGGCGGTCTTTTAAGTCTGATGTGAAAGCCCACGGCTCAACCGNGGAGGGTCATTGGAAA CTGGAGGACTTGAGTGCAGAANANGAGAGTGGAATTCCACGTGTAGCGGTGAAATGCGTAG ATATGTGGAGGAACACCAGTGGCGAAGGCGGCTCTCTGGTCTGTAACTGACGCTGAGGCGC GAAAG) with total sequenced 218 bp.

The photo images of the branches stained with methylene blue are compared in Fig. 8. Methylene blue staining is based on the cation-anion binding between the sample and the pigment, which makes it especially fitting for carrageenan and other anionic hydrocolloids (Soedjak 1994; Campo et al. 2009). It is rather difficult to recognize, but seems that the carrageenan concentration is lowest in the branch with the orange bacteria (b) compared to the other two samples.

Discussion

The increment of reducing sugar (Fig. 2b) was observed in the sample with carrageenan as the only carbon source in the culturing media. This reveals that the red and orange bacteria are able to produce enzymes to hydrolyze carrageenan into reducing sugars such as di- or penta-galactose. *k*-Carrageenase endohydrolases that cleave the internal b-(1-4) linkages of carrageenan yielding oligogalactans which cleaving possible bonds at Degree polymerization (DP) 4s and DP2s (Chauhan and Saxena, 2016) The two bacteria showed different growth rate curves, may be due to the difference in the ability to digest carrageenan between the red and orange bacteria. At the beginning of the experiment, the curves indicate that there was no or little enzyme produced by the bacteria as a decrease of inherent reducing sugar during the first 2 days incubation. It is worth to note that the enzymatic reaction was not observed without the presence of bacterial cells. Since the bacteria were removed by centrifugation, it is assumed that the bacterial body has not been destroyed. This suggests that the bacteria digest carrageenan outside of their cells by secretion of the enzyme but not incorporating carrageenan into the cell. It should be noted that the bacterial population did not increase even after the 3rd day even though the enzyme had produced reducing sugars. Intriguingly, this result suggests that the infectious capability of the bacteria used in this study is very low towards seaweeds that accumulate carrageenan as their energy reservoir.

Red and orange bacteria are successfully identified by 16S rDNA gene sequencing. Red bacteria was identified with high possibility as *Bacillus vietnamensis* with the percent of similarity is up to 99%. On the other hand, the orange bacteria was identified as *Bacillus hwajinpoensis* with percent of similarity is up to 98%. The Global Catalog of Microorganism reported that *B. vietnamensis* is isolated from mangrove sediment while *B. hwajinpoensis* is isolated from seaweed. Chauhan and Saxena (2016) was reported that several bacterial from genus Bacillus was able to produce carrageenase.

To study the bacterial enzymatic carrageenan degradation activity in the algal body, the Raman image technique was employed. The present sample of algal body had a low fluorescent background as shown in Fig. 3(a). The *K. alvarezii* is a red alga rich in phycoerythrin, carotenoids, and chlorophylls for photosynthesis (Indriatmoko et al. 2015). In contrast, the sun-dried seaweed samples possessed less color. This suggests that the photosynthetic pigments have been destroyed by the exposure of ultraviolet light in sunlight. The spectrum of the algal body in Fig. 3(a) does not have bands at 1735 and 1660 cm-1, bands that usually represent lipid and protein, suggesting that these materials also have decomposed during the sun-drying procedure. The algae samples have a high content of carrageenan and small main-body structure of cellulose. The spectra in the hyperspectral images were normalized to a band at 1470 cm^{-1}. The band is assigned to CH bending mode that is present for almost all organic materials. Especially in bioorganic materials, the intensity of this band represents the amount of carbon, as there are few double and triple bonds in bio-molecules. The PLSR calibration model to predict carrageenan concentration was built with the 11 test samples of mixed powders of carrageenan and cellulose. Therefore, water was not taken into account in the present analysis.

The PLSR calibration curve had high correlation coefficient (R^2), although it was built with only first component. The model was applicable to the present samples. Concentration maps of carrageenan were successfully composed from the dataset of 3D Raman images of the slice. The maps indicate that carrageenan is localized heterogeneously in the algal body. A similar distribution of carrageenan seems to be observed in the picture of methylene blue stained branch, but this is not quite clear. Since the Raman image system possess confocal optical configuration, it has a high spatial resolution that seems to increase the contrast in the carrageenan concentration map. The sample with orange bacteria showed the largest decrease of carrageenan concentration

after 5 days of incubation. The 3D images indicate that the decrease of the carrageenan concentration was to equal throughout the algal body. However, outside to inside invasion was not shown. This result indicates that the bacteria actively penetrate into the algal body at first, and then start consuming carrageenan. A decrease of carrageenan content was previously observed in algae with *ice-ice* disease (Mendoza et al. 2002). By using the methods and techniques developed in this study, Raman image techniques combined with PLSR analysis of reduced test samples, it seems possible to investigate the way of infection and proliferation of *ice-ice* pathogens in *K. alvarezii*.

Conclusion

The Raman image technique was successfully applied to study the bacterial activity in the algal body. It was possible to measure the Raman spectrum of the sun-dried algae sample without any fluorescent interference. The PLSR prediction model built with only 11 test samples was effective in the quantitative analysis of carrageenan concentration in the algal body. The accumulation of carrageenan is not homogeneous, but rather localized in the algal body. The isolated orange bacterium was able to penetrate into the algal body quickly and degrades carrageenan by secreting hydrolyzing enzymes. The presented results demonstrate that the Raman image technique combined with PLSR analysis has enormous potential in the study of seaweed disease and carrageenan production in algae.

References

Ask EI, Batibasaga A, Zertuche-González JA, San M de (2003) Three decades of Kappaphycus alvarezii (Rhodophyta) introduction to non-endemic locations. Proceedings of the 17th International Seaweed Symposium, South Africa, pp 49-57.

Azevedo G, Hilliou L, Bernardo G, Pinto IS, Adams RW, Nilsson M, Villanueva RD (2013) Tailoring kappa/iota-hybrid carrageenan from *Mastocarpus stellatus* with desired gel quality through pre-extraction alkali treatment. J of Food Hydrocol 31: 94–102.

Barbeyron T, Michel G, Potin P, Henrissat B, Kloareg B (2000) Iota-carrageenases constitute a novel family of glycoside hydrolases, unrelated to that of kappa-carrageenases. J Biol Chem 275: 35499–505.

Blanco-Pascual N, Alemán A, Gómez-Guillén MC, Montero MP (2014) Enzyme-assisted extraction of κ/ι-hybrid carrageenan from Mastocarpus stellatus for obtaining bioactive ingredients and their application for edible active film development. Food Funct 5: 319.

Case RJ, Longford SR, Campbell AH, Low A, Tujula N, Steinberg PD, Kjelleberg S (2010) Temperature induced bacterial virulence and bleaching disease in a chemically defended marine macroalga. Environ Microbiol 13(2): 529–537.

Cunha L, Grenha A (2016) Sulfated seaweed polysaccharides as multifunctional materials in drug delivery applications. Mar Drugs 14:42.

Chauhan PS, Saxena A (2016) Bacterial carrageenases: an overview of production and biotechnological applications. 3 Biotech 6: 146.

Distel DL, Morrill W, MacLaren-Toussaint N, Franks D, Waterbury J (2002) Teredinibacter turnerae gen. nov., sp. nov., a dinitrogen-fixing, cellulolytic, endosymbiotic gamma-proteobacterium isolated from the gills of woodboring molluscs (Bivalvia: Teredinidae). Int J Syst Evol Microbiol 52: 2261–2269.

Goecke F, Labes A, Wiese J, Imhoff J (2010) Chemical interactions between marine macroalgae and bacteria. Mar Ecol Prog Ser 409: 267–299.

Indriatmoko, Heriyanto, Limantaraa L, Brotosudarmo HTP (2015) Composition of photosynthetic pigments in a red alga *Kappaphycus alvarezi* cultivated in different depths. Procedia Chemistry 14:193 – 201.

Karsten U, Bischof K, Wiencke C (2001) Photosynthetic performance of Arctic macroalgae after transplantation from deep to shallow waters. Oecologia 127: 11–20.

Largo DB, Fukami K, Nishijima (1995b) Occasional pathogenic bacteria promoting ice-ice disease in the carrageenan-producing red algae Kappaphycus alvarezii and Eucheuma denticulatum (Solieriaceae, Gigartinales, Rhodophyta). J Appl Phycol 7(6): 545-554.

Largo DB, Fukami K, Nishijima (1999) Time-dependent attachment mechanism of bacterial pathogen during ice-ice infection in Kappaphycus alvarezii (Gigartinales, Rhodophyta). J Appl Phycol 11(1): 129-136.

Largo DB, Fukami K, Nishijima T, Ohno M (1995a) Laboratory-induced development of the ice-ice disease of the farmed red algae Kappaphycus alvarezii and Eucheuma denticulatum (Solieriaceae, Gigartinales, Rhodophyta). J Appl Phycol 7: 539-543.

Lechat H, Amat H, Mazoyer J, Gallant DJ, Buléon A, Lahaye M (1997) Cell wall composition of the carrageenophyte Kappaphycus alvarezii (Gigartinales, Rhodophyta) partitioned by wet sieving. J Appl Phycol 9: 565–572.

Lemoine M, Nyvall Collén P, Helbert W (2009) Physical state of kappa-carrageenan modulates the mode of action of kappa-carrageenase from Pseudoalteromonas carrageenovora. Biochem J 419: 545–553.

Mahardika A, Susanto AB, Pramesti R, Matsuyosh H, Andriana BB, Matsuda Y, Sato H (2018) Application of imaging Raman spectroscopy to study the distribution of Kappa carrageenan in the seaweed *Kappaphycus alvarezii*. J Appl Phycol 30: 1-8.

Malfait T, Van Dael H, Van Cauwelaert F (1987) Raman spectroscopic analysis of the sodium salt of kappa-carrageenan and related compounds in solution. Carbohydr. Res. 163: 9–14.

Mendoza WG, Montaño NE, Ganzon-Fortes ET, Villanueva RD (2002) Chemical and gelling profile of ice-ice infected carrageenan from Kappaphycus striatum (Schmitz) Doty "sacol" strain (Solieriaceae, Gigartinales, Rhodophyta). J Appl Phycol 14: 409.

Necas J, Bartosikova L (2013) Carrageenan: A review. Vet Med 58(4):187–205.

Pereira L, Amado AM, Critchley AT, van de Velde F, Ribeiro-Claro PJA (2009) Identification of selected seaweed polysaccharides (phycocolloids) by vibrational spectroscopy (FTIR-ATR and FT-Raman). Food Hydrocoll 30:1-7.

Pereira L, Gheda SF, Ribeiro-Claro PJA (2013) Analysis by vibrational spectroscopy of seaweed polysaccharides with potential use in food, pharmaceutical, and cosmetic industries. Int J Carbohydr Chem. 2013: 7p.

Pereira L, Gheda SF, Ribeiro-Claro PJA (2013) Analysis by vibrational spectroscopy of seaweed polysaccharides with potential use in food, pharmaceutical, and cosmetic industries. Int J Carbohydr Chem 2013: 7p.

Pereira L, Sousa A, Coelho H, Amado AM, Ribeiro-Claro PJA (2003) Use of FTIR, FT-Raman and 13C-NMR spectroscopy for identification of some seaweed phycocolloids. Biomol Eng 20:223-228.

Potin P, Richard C, Barbeyron T, Henrissat B, Gey C, Petillot Y, Forest E, Dideberg O, Rochas C, Kloareg B (1995) Processing and hydrolytic mechanism of the cgkA-encoded κ-carrageenase of Alteromonas carrageenovora. Eur J Biochem 228: 971–975.

Rhein-Knudsen N, Ale MT, Meyer AS (2015) Seaweed hydrocolloid production: An update on enzyme assisted extraction and modification technologies. Mar Drugs 13: 3340-59.

Rodrigues D, Sousa S, Silva A, Amorim M, Pereira L, Rocha-Santos TA, Gomes AM, Duarte AC, Freitas AC (2015) Impact of enzyme- and ultrasound-assisted extraction methods on biological properties of red, brown, and green seaweeds from the central west coast of Portugal. J Agric Food Chem 63(12): 3177-3188.

Teixeira dos Santos CA, Páscoa RNMJ, Lopes JA (2017) A review on the application of vibrational spectroscopy in the wine industry: from soil to bottle. Trend Anal Chem 88: 100-118.

Toohey BD, Kendrick GA (2007) Survival of juvenile Ecklonia radiata sporophytes after canopy loss. J Exp Mar Biol Ecol 349: 170–182.

Varadarajan SA, Ramli N, Ariff A, Said M, Yasir SM (2009) Development of high yielding carragenan extraction method from Eucheuma Cotonii using cellulase and Aspergillus niger. In Proceedings of Prosiding Seminar Kimia Bersama UKM-ITB VIII, Bangi, Malaysia, pp. 461–469.

Weiner RM, Taylor LE, Henrissat B, Hauser L, Land M, Coutinho PM, et al. (2008) Complete genome sequence of the complex carbohydrate-degrading marine bacterium, Saccharophagus degradans strain 2-40T. PLoS Genet 4: e1000087.

Figures

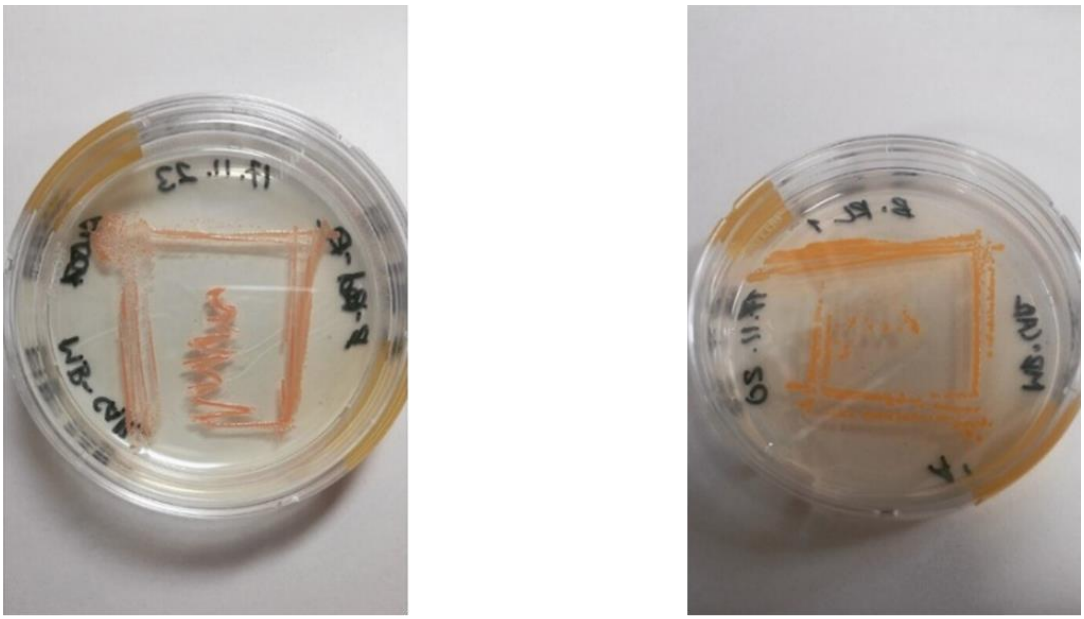

(a) (b)

Fig. 1. Isolated red (a) and orange (b) bacteria from decomposed seaweed.

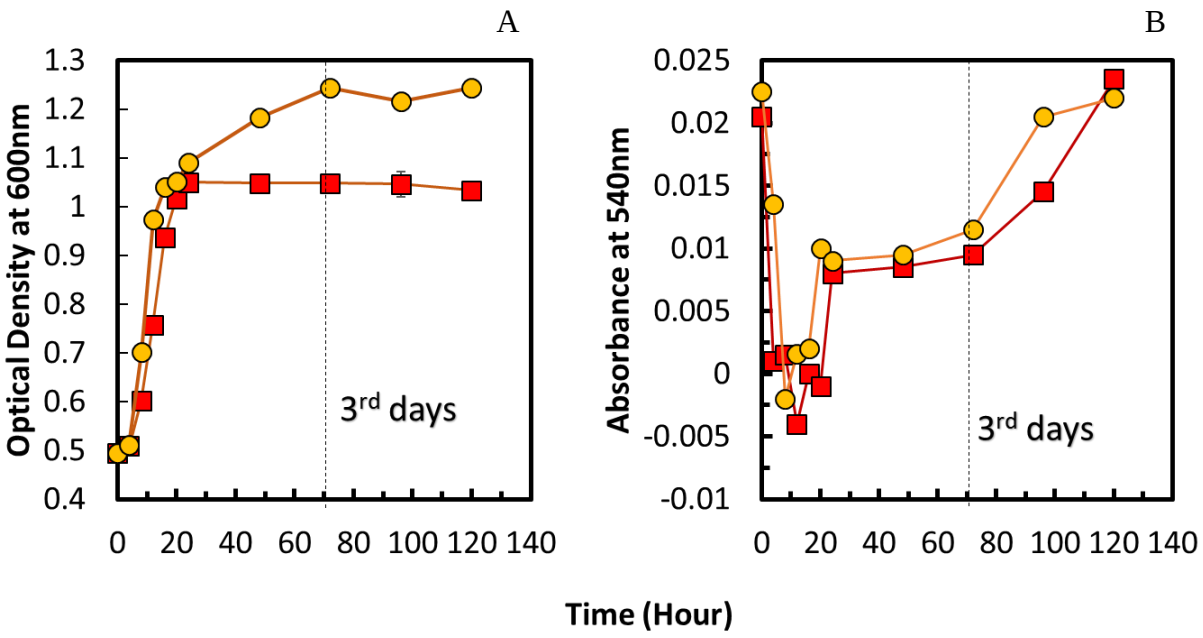

Fig. 2. Growth rate curves (A) of red (red square) and orange (orange circle) bacteria estimated with absorbance at 600 nm and their enzymatic activity curves (B) measured by Miller's method (absorbance at 540 nm).

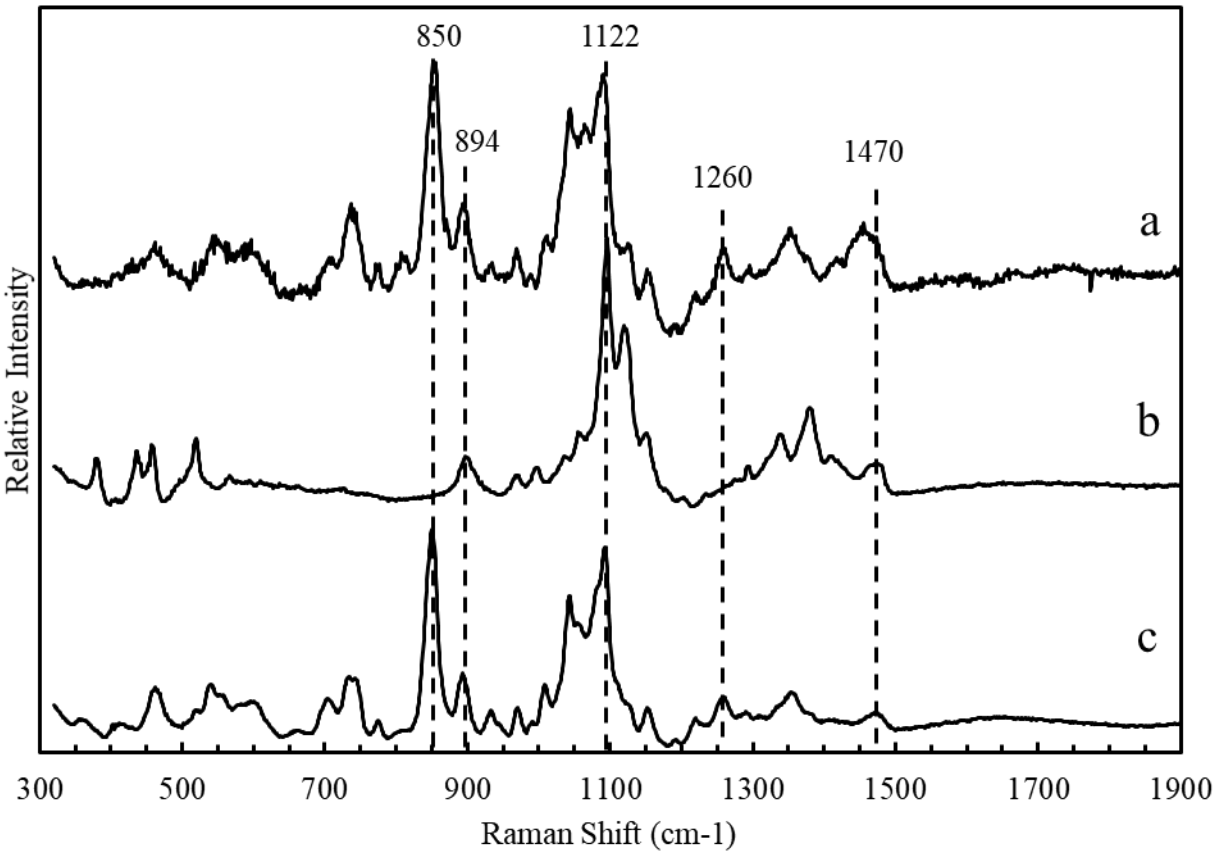

Fig. 3. Raman spectra of thallus of *K. alvarezii* (a), pure cellulose (b), and pure *k*-carrageenan (c).

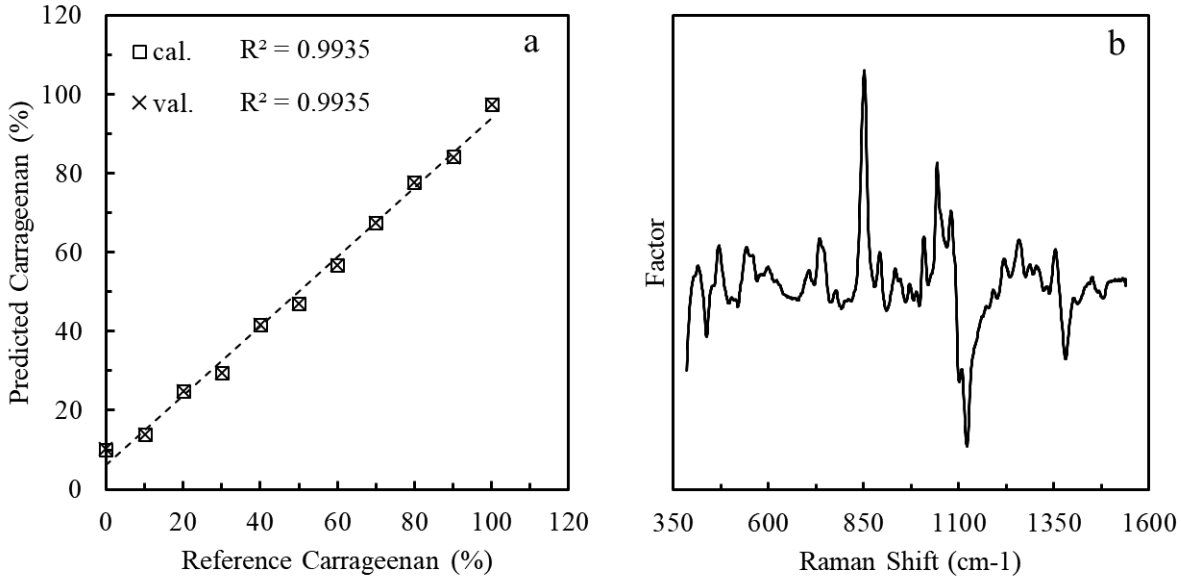

Fig. 4. Calibration curve of the PLSR prediction model for cellulose-carrageenan mixed test samples (a) and the loading plot of factor 1 (b).

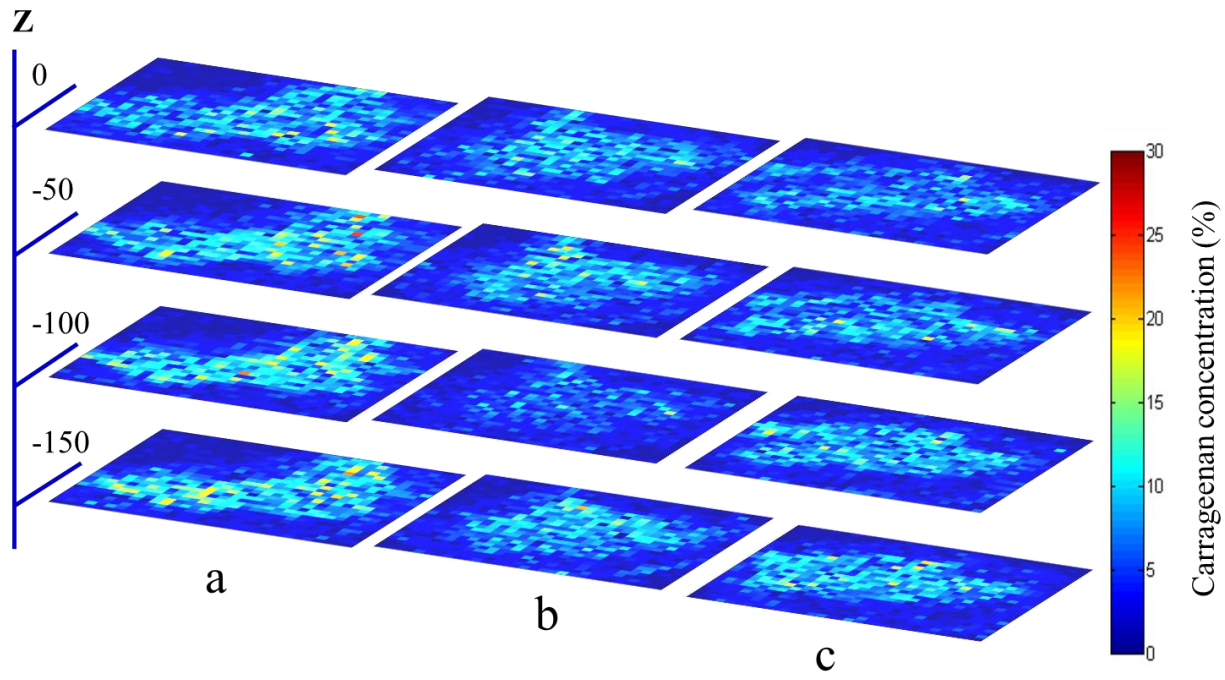

Fig. 5. Raman images of carrageenan distribution in *K. alvarezii* thalli after 3 days incubation with no bacteria (control; a), orange (b) and red (c) bacteria.

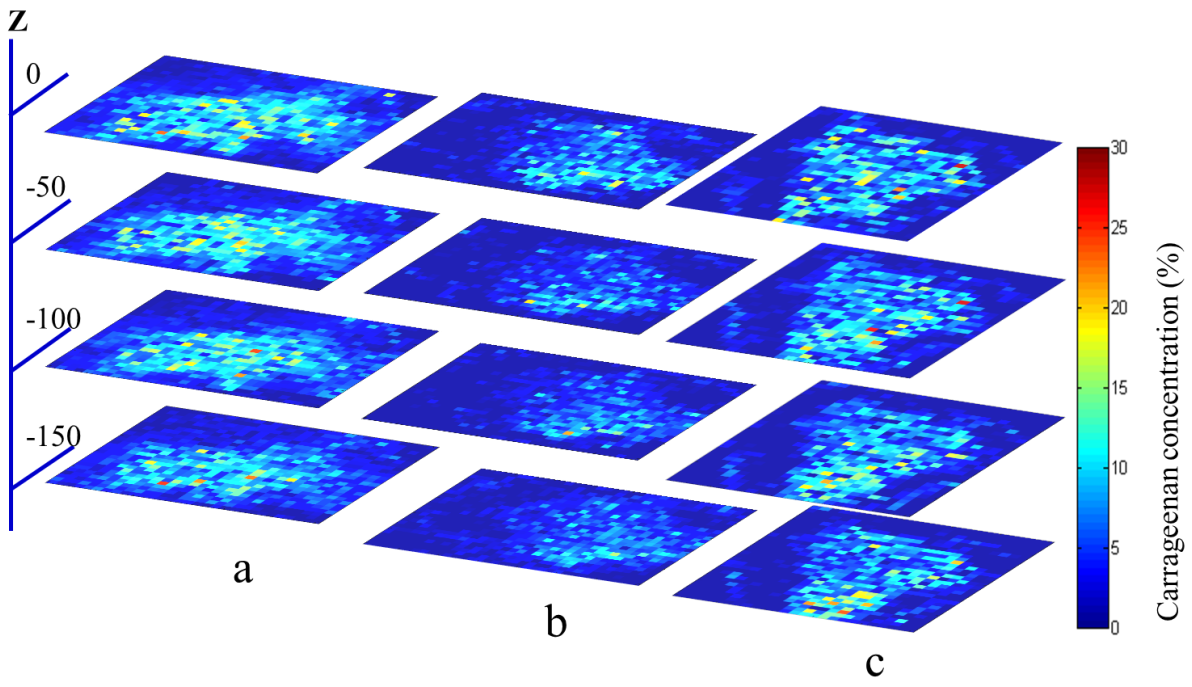

Fig. 6. Raman images of carrageenan distribution in *K. alvarezii* thalli after 5 days incubation with no bacteria (control; a), orange (b) and red (c) bacteria.

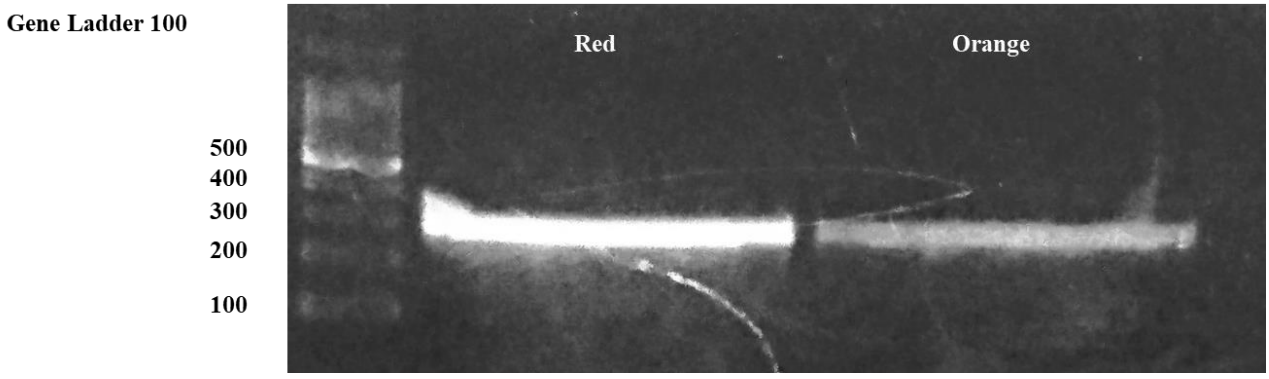

Fig. 7. Gel electrophoresis of 16S rDNA gene amplification

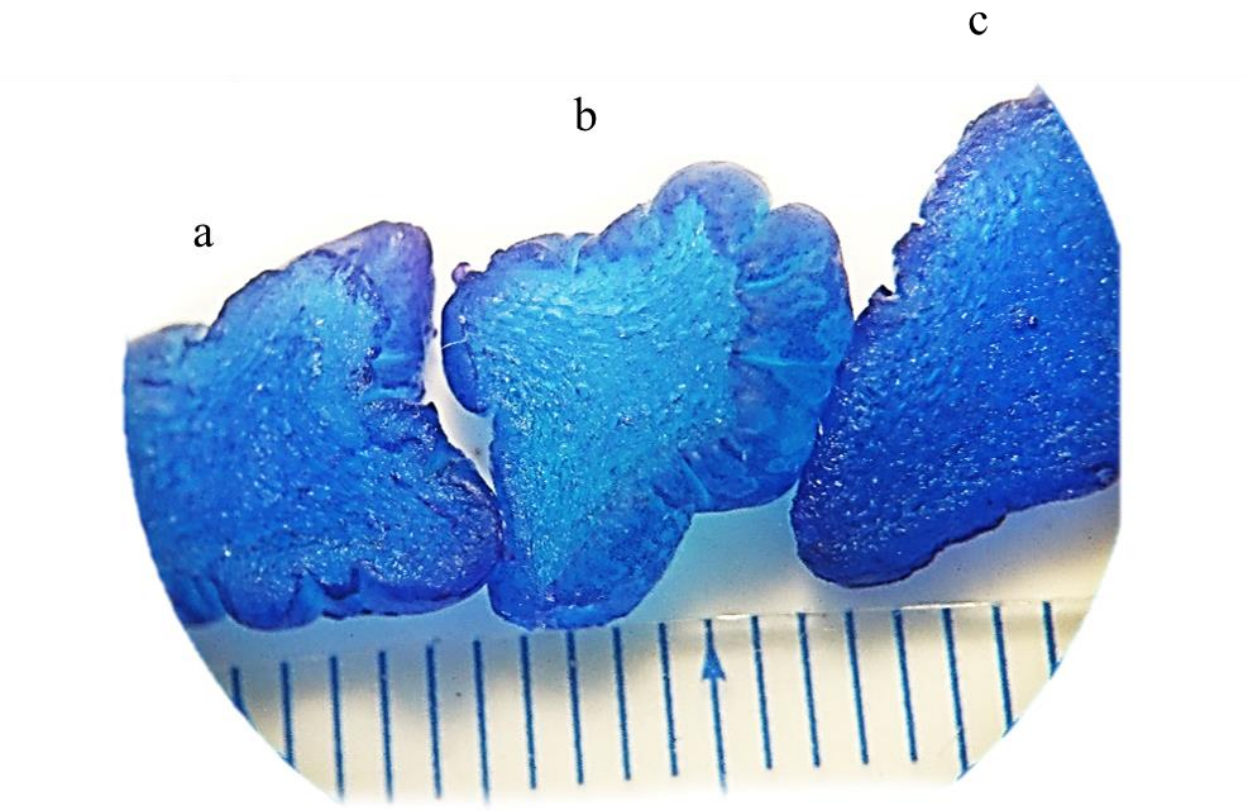

Fig. 8. Photo images of *K. alvarezii* thalli stained with methylene blue after 5 days incubation with no bacteria (control; a), orange (b) and red (c) bacteria.

Wavenumbers (cm^{-1})	Bond(s)/group(s)	Letter code	Kappa
1240–1260	S=O (sulfate ester)		++
1075–1085	C–O (3,6-anydrogalactose)	DA	+++
970–975	Galactose	G/D	+
925–935	C–O (3,6-anydrogalactose)	DA	-
905–907	C–O–SO_4 (C2-3,6-anydrogalactose)	DA2S	-
890–900	Unsulfated β-D-galactose	G/D	-
867–871	C–O–SO_4 (C6-galactose)	G/D6S	-
845–850	C–O–SO_4 (C4-galactose)	G4S	++
825–830	C–O–SO_4 (C2-galactose)	G/D2S	-
815–825	C–O–SO_4 (C6-galactose)	G/D6S	-
804–808	C–O–SO_4 (C2-3,6-anydrogalactose)	DA2S	-

adapted and modified from Pereira, 2009

Table 1. Characterization of κ-type carrageenan by Raman spectroscopy.

No	Carrageenan (%)	Cellulose (%)
1	0	100
2	10	90
3	20	80
4	30	70
5	40	60
6	50	50
7	60	40
8	70	30
9	80	20
10	90	10
11	100	0

Table 2. PLSR model, mixture carrageenan and cellulose

List of Publication

Paper

1. Mahardika A, Andriana BB, Susanto AB, Matsuyoshi H, Sato H (2018) EXPRESS: Development of Quantitative Analysis Techniques for Saccharification Reactions Using Raman Spectroscopy. Appl Spectrosc 72 (11): 1606-1612.

2. Mahardika A, Susanto AB, Pramesti R, Matsuyoshi H, Andriana BB, Matsuda Y, Sato H. (2018) Application of Imaging Raman Spectroscopy to study the Distribution of Kappa Carrageenan in the Seaweed *Kappaphycus alvarezii*. J Appl Phycol.

   https://doi.org/10.1007/s10811-018-1618-8

Conference

1. Anggara Mahardika and Hidetoshi Sato. 2016. Application of Light Spectroscopy for Monitoring Immobilization Enzyme in Organic Material. Poster publication in Japan-Taiwan Medical Spectroscopy International Symposium.

2. Anggara Mahardika, Bibin B. Andriana, Hiroko Matsuyoshi, AB Susanto, Hidetoshi Sato. 2017. Development of Quantitative Analysis for Monitoring Saccharification Process Using Raman Spectroscopy. Poter publication in ICAVS 9th, Canada.

3. Anggara Mahardika, Kouki Nakamura, Yusuke Matsuda, Hidetoshi Sato. 2017. Raman spectroscopy for monitoring enzymatic reaction of immobilized enzyme on diatom Thalassiosira pseudonana silica cell wall. Poster pubilcation in Molecular Life Diatom, Japan.

4. Anggara mahardika, A.B. Susanto, Rini Pramesti, Yusuke Matsuda, Hidetoshi Sato. 2017. Quantitative analysis of saccharides in Kappaphycus alvarezii using Raman Imaging. Poster publication in SCIX, Nevada.

5. Anggara Mahardika, A.B. Susanto, Rini Pramesti, Hiroko Matsuyoshi, Yusuke Matsuda, Hidetoshi Sato. 2018. Study of Carrageenan Concentration and Distribution in Seaweed Kappaphycus alvarezii using Raman 3D imaging and Chemometric Analysis. Poster Presentation in ICAMS. Japan.

Acknowledgment

First of all I would like to be grateful to my Lord Jesus Christ for the guidance, accompaniment, and strengthening me during my study in doctoral program. I would like to express my sincere gratitude to my advisor Prof. Hidetoshi Sato, Prof. Bibin Bintang Andriana, and Dr. Rer. Nat. AB Susanto for the continuous support of my Ph.D. study and related research, for his patience, motivation, and immense knowledge. His guidance helped me in all the time of research and writing of this thesis. I could not have imagined having a better advisor and mentor for my Ph.D. study. Besides my advisor, I would like to thank the rest of my thesis committee: Prof. Yusuke Matsuda and Prof. Hiroyuki Toh for their insightful comments and encouragement, but also for the hard question which incented me to widen my research from various perspectives. My sincere thanks also goes to Prof. Shinsuke Fujiwara who provided me an opportunity to join their team as intern, and who gave access to the laboratory and research facilities. Without they precious support it would not be possible to conduct this research. I thank my fellow labmates in for the stimulating discussions, for the sleepless nights we were working together before deadlines, and for all the fun we have had in the last three years. Last but not the least, I would like to thank my family: my parents, my beloved wife and my beloved daughter also to my brothers for supporting me spiritually throughout writing this thesis.